Summer 2017

Nocturnal Drying in Elevated Coastal Terrain of Central California: A Fire Weather Perspective

Richard Bagley
San Jose State University

NOCTURNAL DRYING IN ELEVATED COASTAL TERRAIN OF CENTRAL CALIFORNIA: A FIRE WEATHER PERSPECTIVE

A Thesis

Presented to

The Faculty of the Department of Meteorology and Climate Science

San José State University

In Partial Fulfillment

of the Requirements for the Degree

Master of Science

by

Richard Bagley

August 2017

The Designated Thesis Committee Approves the Thesis Titled

NOCTURNAL DRYING IN ELEVATED COASTAL TERRAIN OF CENTRAL CALIFORNIA: A FIRE WEATHER PERSPECTIVE

by

Richard Bagley

APPROVED FOR THE DEPARTMENT OF METEOROLOGY AND CLIMATE SCIENCE

SAN JOSÉ STATE UNIVERSITY

AUGUST 2017

Dr. Craig B. Clements	Department of Meteorology and Climate Science
Dr. Sen Chiao	Department of Meteorology and Climate Science
Dr. Neil Lareau	Department of Meteorology and Climate Science

ABSTRACT

The second largest fire shelter deployment in U. S. history occurred during the Devil Fire in a remote and rugged region of the San Francisco Bay Area when relative humidity values abruptly dropped in the middle of the night, causing rapid fire growth. Nocturnal drying in the higher elevations along California's central coast is a unique phenomenon that poses a great risk to firefighters. Single digit relative humidity with dew points below -25°C is not uncommon during summer nights in this region. In order to provide the firefighting community with knowledge of these hazardous conditions, an event criterion was established to develop a climatology of nocturnal drying and investigate the synoptic patterns surrounding such episodes. Furthermore, a detailed case study of the Devil Fire incident, including a high resolution numerical simulation, was used to understand the interaction between complex topography, the boundary layer, and a subsidence inversion. A lower tropospheric source region of dry air was found over the northeastern Pacific, corresponding to an area of maximum low-level divergence and associated subsidence. This dry air forms above a marine inversion and advects inland with the marine layer through gaps in the coastal barrier overnight. As the boundary layer over higher terrain collapses at night, the inversion lowers and immerses upper slopes with warm and dry air. An average of 15-20 nocturnal drying events per year occur in elevations greater than 700 m in the San Francisco Bay Area and their characteristics are highly variable, making them a challenge to forecast.

ACKNOWLEDGEMENTS

I would like to express gratitude to my thesis committee for their help and guidance in writing this thesis. I would like to thank my advisor, Dr. Craig Clements for all the support with my research as well as the motivation to see it through. I would also like to thank the other members of my committee, Dr. Neil Lareau and Dr. Sen Chiao for their comments and suggestions for improving my thesis.

I would also like to acknowledge former Santa Clara Unit Battalion Fire Chief Dave MacLean for the knowledge to initiate this study. Also, a special thanks to my fellow students for their help at various stages of my research. Finally, I would like to thank my wife, Allison, for her support, advice, and especially patience throughout this process.

TABLE OF CONTENTS

.

LIST OF TABLES

LIST OF FIGURES

1. Introduction

The amount of moisture in the atmosphere has long been recognized for its contribution to fire behavior. Munns (1921) related the amount of evaporation to the size of forest fires in the San Bernardino Mountains and showed how the occurrence and spread of large fires coincided with increased rates of evaporation or a decrease in vapor pressure. A similar study by McCarthy (1923) in the southern Appalachian Mountains found that low vapor pressure is usually accompanied by low relative humidity (RH) and is therefore an indicator of fire hazard when used in conjunction with temperature.

In addition to moisture, wind and air temperature comprise the three key meteorological variables inextricably linked to fire behavior. Their connection to weather patterns was first established by Beals (1914) who identified synoptic pressure gradients associated with strong winds and large fires. Schroeder et al. (1964) wrote the original catalogue of critical U. S. fire weather scenarios, comparing four common upper-air patterns (meridional, zonal, blocking, and short-wave train) to their associated critical fire weather component. He further divided the contiguous 48 states into 14 separate regions to show the more localized effects of these patterns. The two regions encompassing California shared similar synoptic patterns, with the four most critical being a subtropical high aloft, a meridional ridge with southwesterly flow, a post-frontal Pacific High, and the Great Basin High. The subtropical high aloft was responsible for the most number of high fire danger days in the region because of intense warming, effectiveness in blocking moisture, and frequency of occurrence. The great Basin High was recognized as the most critical pattern because of its role in producing the Santa Ana

winds associated with strong offshore flow and low RH. The other two synoptic patterns, which generally correspond to the periphery of a high pressure system, were acknowledged by their tendency to produce northerly winds over the state.

Brotak and Reifsnyder (1977) examined the synoptic situations of fifty-two fires from the eastern half of the United States and found that most rapid rates of spread occur immediately behind a dry cold front in the southeastern section of a high pressure area. Moisture advection at 850 hPa was also insufficient to allow for precipitation in 93% of these cases, yet the dynamics still favored regions of strong winds. Similarly, Nimchuk (1983) stated that while an upper ridge corresponds to warmer and drier conditions, extreme fire behavior is triggered by decreased stability and an increase in winds as this ridge breaks down.

Several more recent studies have been conducted to investigate the role between synoptic conditions and the exchange of extremely dry air between the upper troposphere and the surface. Zimet et al. (2007) discuss the meteorology behind the Mack Lake wildfire in Michigan that began as a prescribed burn, but lost containment and eventually burned 24,000 acres in 30 hours. An upper-level front embedded within northwesterly flow of a short wave trough over central Canada was deemed responsible for the fire's explosive growth. Ageostrophic adjustment at the jet exit region intensified the front and enhanced descent upstream of the fire. The associated subsidence ushered in dry air from the upper to lower troposphere along the sloping isentropes behind the front.

Similar conditions were noted by Kaplan et al. (2008) during the Double Trouble fire in coastal central New Jersey when rapid growth coincided with RH values less than 20%

and surface winds of 17 m s^{-1}. Like the Mack Lake fire, a thermally indirect circulation of the right exit region of a jet streak was responsible for transporting high momentum and extremely dry air to the mid-troposphere. The drying process during the Double Trouble fire was considered two-fold and involved the presence of a weak surface cold front. An initial drying event occurred from the passage of a dry cold front and low-level isallobaric divergence. A second drying event occurred as daytime heating deepened the mixing layer and coupled dry air from the descending branch of the indirect circulation with the convective boundary layer.

A similar extreme reduction in surface humidity (< 10%) was observed during two separate devastating southern Australia fires in 2003 and 2005 (Mills 2008a, 2008b). Like Zimet et al. (2007) and Kaplan et al. (2008), Mills (2008a) found a two part process responsible for transporting dry upper-tropospheric air to the surface. The first phase consisted of jet stream entrance and exit circulations that brought upper-level dry air into the mid-troposphere. The second phase included a deep and well-mixed boundary layer through which dry convection entrained low humidity air to near-surface levels. While the first phase lasted for hours, the second phase of boundary layer mixing took place in less than an hour. Satellite water vapor imagery was also used to identify the dark band of dry air associated with subsidence and cross frontal circulations during drying events.

Mills (2008b) also conducted a preliminary climatology of southern Australia drying events spanning six fire seasons. A drying event was categorized as having dew points less than - 5°C or dew points less than -2.5° and RH less than 10%. To further refine event abruptness, an event score was based on dew point variance, range, and deviation.

Two hundred and thirty-two drying events were compiled from 18 different stations. Most events occurred between mid-morning and early evening (LST). A strong spatial and temporal coherence was identified with nearby stations simultaneously reporting drying event criteria, indicative of large-scale forcing. For each event, a subjective assessment of satellite water vapor imagery concluded that 60% of the cases exhibited a dark band of dry air, with 80% being on the peripheral of this dry band. Heights at the 300 hPa level and wind analyses suggest that a large portion of these drying events correspond to anticyclonic shear and curvature.

While the aforementioned synoptic studies include processes that transport high momentum, dry air from the upper troposphere to the near-surface, there are other drying scenarios that involve a lower tropospheric source origin. One of the more recognized examples would be the Santa Ana winds of southern California, a hot, dry, foehn-like wind that originates in the Great Basin of the western U. S. and flows southwestward through mountain gaps into coastal southern California (Whiteman 2000). Most typical between fall and spring, Santa Ana winds develop from an anticyclone over Nevada, Utah, and Northern Arizona with adjacent low pressure off the California coast (Schroeder et al. 1964). The pressure gradient sets up northeasterly flow that compresses and warms adiabatically as it descends into lower elevations. Some of the more extreme Santa Ana cases are capable of winds gusting up to 50 m s^{-1} and RH values below 10% (Sommers 1978).

The Cedar fire of 2003 was the largest fire in California state history and occurred during a more complicated Santa Ana event. Huang et al. (2009) diagnosed the synoptic

and mesoscale features surrounding this rare fire event using observational data and numerical simulations. Of primary influence was an upper-level ridge over the northwest U. S., with a jet streak on its northeast boundary and a trough digging downstream over the central U. S. Subsidence corresponding with the ageostrophic circulation about the jet exit region first established a dry air source in the upper-levels. As the trough deepened, strong northeasterly flow advected dry air southwestward towards the California coast. Finally, the boundary layer was coupled with the dry air aloft through a wave-induced critical level that led to the formation of a hydraulic jump over the near-coastal topography, creating Santa Ana winds.

Large-scale weather patterns and upper-level features have proven critical to the development of momentum, temperature, and moisture characteristics within the boundary layer that directly affect fire behavior (Werth et al. 2011). Much of the previous discussion involves the translation of extremely dry, high-momentum air from the upper troposphere to the near-surface. While California is subject to this type of atmospheric behavior, there exists a unique phenomenon in which extremely dry air above the marine layer is ushered into the upper elevations of coastal California. Coincidentally, the development of this dry air source is intricately linked to the formation of coastal stratus and fog in the northeastern Pacific marine atmospheric boundary layer (MABL) during summertime.

Across the northeastern Pacific, an inversion with a base at 2 km over the Hawaiian Islands gradually slopes eastward and reaches its lowest point of 400 m along the California coast (Neiburger 1960). A semi-permanent anticyclone centered near 38°N

and 150°W is responsible for this large-scale feature through subsidence and low-level divergence along its eastern boundary. The resultant winds in this region deviate from the geostrophic wind, spiraling outward from the anticyclone diverging southwestward and parallel to the California coast. In addition to streamline divergence, an increase in winds outward from the high pressure center combine to create a maximum in divergence along the California coast.

While Neiburger (1960) found small values of vertical velocities over the eastern Pacific, the associated horizontal values are also small and imply that the gradual sinking of air takes place over an extended period of time as it moves around the anticyclone. The trajectories of air from San Francisco and Los Angeles at 600 m calculated backward to the 700 hPa level both showed an origin to the north and east of the high pressure center. The trajectories also had the most rapid rate of descent in the vicinity of the coast (Neiburger 1960).

The prevailing north-northwesterly flow along the U. S. west coast is the primary mechanism for fog and status production as well as the corresponding capping inversion. The main processes involved in their formation are discussed in detail by Pilié et al. (1979) from shipboard measurements along the California coast that confirmed previous theories (Petterssen 1938; Leipper 1948). Initial stratus-free environments occur when offshore winds push dry air out to sea and destroy the moist, unstable MABL. As winds return to their normal direction of 330°, continued subsidence lowers an inversion close to the surface and effectively traps moist air near the ocean-atmosphere interface. According to Pilié et al. (1979), as this layer crosses over spots of warmer water, local

instability initiates condensation and forms cloud or fog patches that align themselves with the direction of the prevailing winds, similar to cloud streets. A local inversion is soon established at the top of these patches through radiative cooling, which in turn decrease low-level stability and develop a well-mixed boundary layer. Gradually, the inversion is lifted off the surface through radiation from several fog patches. Fog-stratus systems over the northeastern Pacific usually develop into a wedge-shaped pattern that widen to the south.

This maritime regime often advects onshore to clash with the warm, dry air mass that occupies the western portion of the U. S. during summertime, creating a boundary in which each are modified. Edinger (1963) studied these transitions over coastal southern California and observed the boundary layer to be neutrally stable along the coast and more stable with complex configurations inland. At around 60 km inland, the marine layer becomes diluted as buoyant air is able to penetrate a weakened inversion. He also noted a dry tongue above the marine layer that was driest and deepest at the coast and became progressively more moist and shallow further inland. Schroeder (1960) and Fosberg (1956) noted various forms of nocturnal drying in the coastal ranges of California above an inversion, but could not identify the source region.

It is the warm, extremely dry air residing above the marine layer that is the focus of this paper as it relates to fire danger. While much research has been devoted to the marine layer off the California coast, relatively little is known concerning the inversion layer above it. Some of the most extensive work on this subject was done by Albert Miller in the 1960's and 1970's whose projects included the Sutro Tower Atmospheric

Boundary Layer Experiments (STABLE) and the Marine Atmospheric Boundary Layer Experiments, West Coast (MABLE WC). Some of his early discoveries, as presented by Lester (1985), include the non-uniform topography of the inversion base height over the San Francisco Bay Area (SFBA), and wave phenomena within the inversion that play an important role in cross-inversion fluxes.

The MABLES WC experiment was conducted in an area extending 200 km from California's central coast using aircraft and shipboard measurements collected at several levels. The results presented by Bridger et al. (1993) support Miller's previous findings that inversions were lower and stronger in the east than the west with base heights and temperatures similar to values observed in the SFBA. Wavelike perturbations in the potential temperature field were also present as evidence of internal gravity waves. Strong vertical wind shear was also observed in the presence of a low-level jet (LLJ) within the inversion layer with speeds over 17 m s^{-1}.

Burke and Thompson (1996) examined the complex dynamics of the LLJ off the California coast using a hydrostatic mesoscale model. Of primary importance in its development is the juxtaposition a synoptic scale pressure difference between an anticyclone to the west and thermal low to the east. Baroclinity is also established between the cold sea-surface and warm continent. Two other sensitivity simulations were run; one that eliminated terrain and another that eliminated zonal SST variation. In both cases, the LLJ remained offshore, proving pressure gradients and baroclinity as their principle driver. A well-developed mixed layer within the MABL keeps the LLJ within the inversion instead of near the surface.

Combined with increased temperatures and lack of moisture, the inversion above a marine layer along coastal California often heralds extreme fire danger in upper elevations. Between 925 and 850 hPa, the subsidence inversion above a west coast marine layer can contain air with mixing ratios as low as 0.5 g kg^{-1} and dew point temperatures below -25°C. The largest fire shelter deployment in California and second largest in U. S. history took place when dry conditions above a marine layer intruded into the upper and northern portions of the Diablo Range in the SFBA where the Santa Clara Complex was actively burning. After midnight on 29 August 2003, crew members battling the Devil Fire were overrun when RH abruptly plunged into the single digits causing extreme fire behavior and the subsequent 53-person shelter deployment.

The counter-intuitiveness of these types of drying events is two-fold. First, the moisture recovery in these upper elevations is opposite of typical trends (Whiteman 2000) and in phase with the diurnal temperature cycle. Relative humidity peaks during the afternoon and is often lowest overnight. Second, these events are usually above a higher moisture environment with stratus clouds or fog, which has the opposite effect on fire activity, and only a thin interface separates the two. The motivation of this research is to understand nocturnal drying as it pertains to fire behavior and fire danger. Firefighting agencies need to be aware of critical fire weather conditions unique to the area and meteorologists must be able to forecast them in a timely manner. This paper first establishes a set of criteria to identify the spatial and temporal extent of nocturnal drying through a climatology of weather stations across California and Oregon where these events are known to occur. A synoptic composite is also used to determine

the source region of dry air and how large-scale momentum, temperature, and moisture variables evolve in the days before and after significant overnight drying.

2. Methods

Local, state, and federal agencies around the SFBA are familiar with summertime overnight drying in higher coastal terrain, but remain unaware of the cause and extent. In order to determine what qualifies as an event, a basic set of threshold criteria was established based on surface meteorological conditions corresponding to the time of extreme fire behavior and subsequent overrunning of the Devil Fire during the night of 29 August 2003. Relative humidity values between 20 and 30% were reported that evening, and then shortly after 0100 PDT, RH suddenly dropped to single digits during the time of deployment. Dew point temperatures also plunged below -10ºC from the onset of explosive fire growth until sunrise. Therefore, a nocturnal drying event (NDE) is hereby identified as a period of at least three hours between 2000 and 0800 PDT during which RH values below 9.5% accompany dew point temperatures less than or equal to -10.0ºC. Such meteorological conditions can be considered critical fire weather associated with extreme fire behavior. Mills (2008) used similar methods involving RH lea than 10% in combination with dew point criteria when evaluating event scores for drying episodes in Australia. Furthermore, the NWS generally establishes a minimum RH threshold below 9 or 10% when determining Red Flag warning criteria. The dew point threshold was used to place added importance on the lack of moisture that drives such low RH values.

2.1 Climatology

A 15-year climatology of NDEs was conducted using data from Remote Automated Weather Stations (RAWS) using Mesowest (Horel at al. 2002). In order to sample as much as the free atmosphere as possible above the marine inversion, 30 stations were selected based on their location atop mountain peaks, ridges, or upper slopes in elevations greater than 450 m (Table 1). Of further importance was station participation in the National Fire Danger Rating System (NFDRS) to ensure quality measurements and records. Of the 30 stations used, 24 are part of the NFDRS. The majority of stations are scattered across California, with the greatest concentration in the SFBA coastal terrain and southern California mountains. Five of the stations are in the Sierra Nevada and three are in western Oregon. For clarity and to distinguish different climatological exposures to the marine layer, sites are grouped into five regions: coastal Oregon (OR), coastal northern California (NC), SFBA, coastal central California (CC), southern California (SC), and Sierra Nevada (SN).

Twelve of the 30 RAWS used in this study have been operable for at least 15 years and only five stations have less than ten years of data. If more than six months of observations were missing from a particular station, that year was excluded from the annual running average. If three or more months were missing from a station between 1 May and 31 October, that year was excluded from the seasonal average. Maximum and minimum values were examined to parse and remove any data extremes that might skew results. Further data quality assurance was performed by visually inspecting annual time series plots of temperature, dew point, and RH for any outlying values.

Table 1. Listing by region of stations used in climatology of NDEs from 2000-2014.

Station (Region)	Elev (m MSL)	Lat (º)	Lon (º)	ID	Event Count May-Oct	Event Count Annual
Coastal Northern California (NC)						
Cooskie Mountain	898	40.26	-124.27	PTE	4	12
Hawkeye	617	38.74	-122.84	HWK	1	4
Mendocino Pass	1640	39.81	-122.95	MAS	2	14
Slater Butte	1409	41.86	-123.35	ATR	2	4
Yolla Bolla	1366	40.34	-123.07	YOB	1	11
San Francisco Bay Area (SFBA)						
Mt. Diablo	1173	37.88	-121.91	MTD	37	49
Rose Peak	933	37.50	-121.74	RSP	22	35
Ben Lomond	792	37.13	-122.17	BND	14	17
Middle Peak	713	37.93	-122.59	MDE	15	27
Atlas Peak	590	38.47	-122.26	ATL	2	7
Big Rock	457	38.04	-122.57	NBR	1	2
Las Trampas	537	38.83	-122.07	LTR	2	3
Diablo Grande	567	37.33	-121.30	DBL	2	3
Los Gatos	561	37.20	-121.95	LSG	4	5
Cordoza Ridge	711	37.17	-121.53	TT119	2	4
Coastal Central California (CC)						
Figueroa	970	34.73	-120.01	FGM	5	23
Highlands Peak	759	36.07	-121.56	HPE	13	28
Southern California (SC)						
Mt Wilson	1740	34.23	-118.07	MWS	27	50
Camp 9	1219	34.35	-118.42	CNI	14	31
Malibu Hills	480	34.06	-118.65	MBU	3	19
Alpine	857	32.84	-116.67	ANE	3	19
Otay Mountain	1001	32.60	-116.84	OTY	13	28
Sierra Nevada (SN)						
Carpenter Ridge	1468	40.07	-121.584	CDE	2	5
Pike County Lookout	1128	39.47	-121.202	PKC	1	3
Duncan	2164	39.14	-120.51	DUC	1	21
Mt Tom	2738	37.38	-119.18	MMT	4	20
Mountain Rest	1253	37.05	-119.37	MTQ	0	1
Oregon (OR)						
Rock House	548	44.93	-123.47	RKH	0	0
Sugerloaf	1319	43.66	-122.63	SGF	1	4
Bald Knob	1106	42.69	-124.04	BKF	1	4

The spatial and temporal extent of nocturnal drying was first identified by establishing an annual and seasonal count of NDEs from all 32 RAWS between 2000 and 2014. A more extensive investigation was then conducted involving four sites from the SFBA. The selected stations are at an elevation above approximately 800 m above mean sea level (MSL), located near or atop a peak or ridge, and spread throughout the SFBA representing an areal coverage of over 3,000 km^2, and include the various mountain ranges surrounding the SFBA (Fig. 2.1). Located at 713 m MSL along a ridge near the peak of Mt. Tamalpais, MDP is the most northwestern site of the four. Farther south, along the coast and above the town of Ben Lomond, BND is situated atop a far western spine of the Santa Cruz Mountains at an elevation of 792 m MSL. Representing the interior mountains of the SFBA are Mount Diablo (MTD) and Rose Peak (RSP). Perched atop the summit of conically shaped Mt. Diablo (1173 m MSL), MTD is the highest and most exposed location of the four RAWS. Rose Peak RAWS is located in an upper, west-facing slope at 933 m MSL in the northern portion of the expansive Diablo Range and is the most sheltered of the four sites.

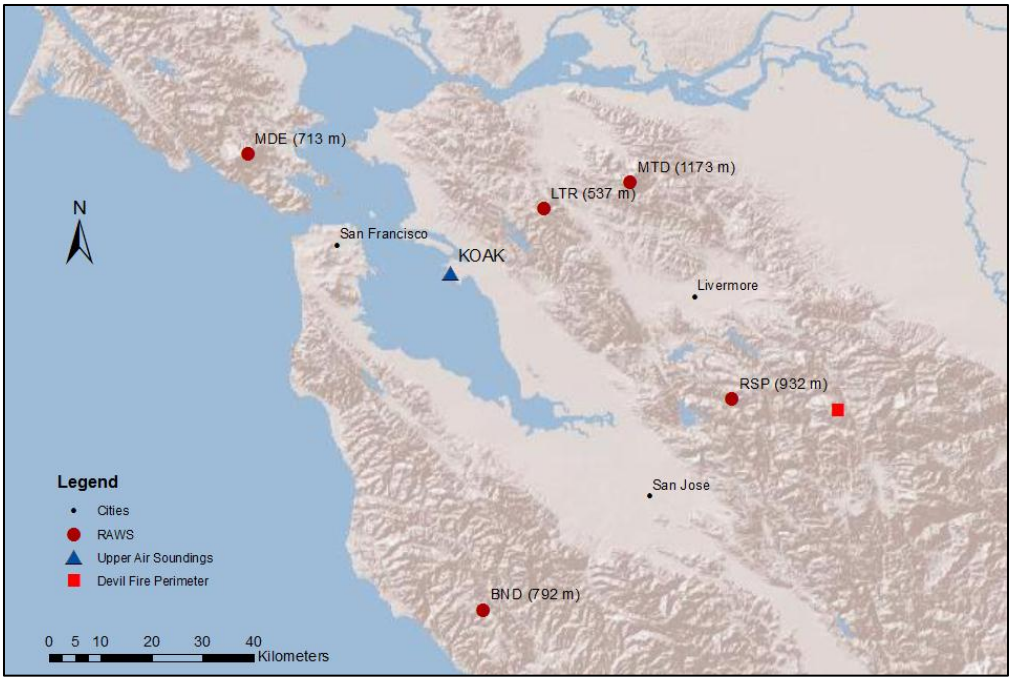

Fig. 2.1. Map of Devil Fire perimeter, four primary SFBA RAWS, and launch site of KOAK upper air soundings.

Data analysis of the selected SFBA stations started with the relative frequency of occurrence of NDEs on daily and seasonal scales. Histograms were constructed of events per month on an annual basis and events per hour on a seasonal basis between 1 May and 31 October. A statistical analysis was then performed on pertinent meteorological variables such as temperature, winds, dew point, and relative humidity to find mean values over the summer, as well as 25th and 75th percentile breakdowns. These were then compared to the mean and maximum (minimum) values of temperature and wind speed (RH and dew point) during NDEs. Similar statistics were performed for measured fuel moisture and fuel temperature. To compare conditions in the sparsely populated higher elevations of the SFBA to a more densely populated area, Las Trampas (LTR) afforded a

good approximation of the wildand-urban interface. Located atop a ridge in the eastern edge of the East Bay Hills, LTR (537 m MSL) is representative of lower elevations and is in the geographic center of the greater SFBA hills and mountains.

2.2 Composite Analysis

a. Pressure levels

There have been instances in which significant overnight drying effects an entire region simultaneously, as well as reaching abnormally low levels. To further understand the circumstances under which more significant NDEs occur, large scale momentum, temperature, and moisture characteristics of the atmosphere were investigated before, during, and after the most critical periods of nocturnal drying in the SFBA spanning an eleven-year period from 2004-2014. The SFBA has an ideal experimental design with a diverse network of RAWS at all elevations, as well as upper air soundings launched twice daily from Oakland International Airport (KOAK) at 0000 (1700 PDT) and 1200 UTC (0500 PDT) (Fig. 2.1). Oakland Airport is situated near the geographic center of the SFBA and is surrounding by the five RAWS used in the statistical analysis. Figure 2.1 shows the topography, four primary weather stations, and centralized balloon launch site used to identify significant SFBA drying events.

For this purpose, significant nocturnal drying events were recognized when 900 hPa dew point temperatures from the 0500 PDT KOAK sounding were less than or equal to -10°C and at least three of the four stations were below the -10°C dew point temperature and 9.5% RH threshold for at least three hours. Or, in addition to 900 hPa KOAK sounding dew point temperatures below or equal to -10°C, if two stations observed

conditions less than -20°C and 5% for at least one hour, then that also qualified as a significant NDE. In all, 87 significant NDEs were recognized.

A time of T=0 was established when overnight RH and dew point temperatures were at their lowest values during a NDE. Each T=0 then had to be converted to the nearest 6 h interval due to the temporal constraints of the North American Mesoscale (NAM) Model analysis used for compositing. From T=0, 12 hour intervals from 36 hours before and 24 hours after each event were used to show synoptic evolution and are hereby identified as T-36, T-24, T-12, T+12, and T+24 as done in Brewer et al. (2012). For cases in which significant nocturnal drying persisted for multiple nights, the first night is considered T=0, while T+12 and T+24 were calculated from the final consecutive night. Using NAM-218 data, composites of these times were created for MSLP, 975, 925, 850, 700, and 500 hPa pressure levels and corresponding meteorological variables.

b. Upper air sounding

Early morning KOAK soundings from 0500 PDT often exhibit the NDE signature of large dew point depressions above a shallow marine layer. Based on previously identified significant NDEs, corresponding 1200 UTC Oakland soundings were used to create a mean vertical profile of temperature, moisture, and wind variables. Data acquired from University of Wyoming was organized into vertically averaged 10 hPa pressure levels with a surface of 1020 hPa and a top of 100 hPa. Stability and low-level flow diagnostics were then performed at heights above and below the inversion.

2.3 Numerical Simulation of the Devil Fire

The Weather Research and Forecasting model version 3.6 (WRF, Skamarock et al. 2008) was used to simulate the meteorological conditions surrounding the overrunning of the Devil Fire on 29 August 2003. The 3-D, non-hydrostatic WRF modeling system uses a terrain-following sigma coordinate system and was configured with three domains using two-way nesting for all experiments. The outermost domain consists of a 900 x 900 km^2 area centered on the Devil Fire with a horizontal resolution of 9 km (Fig. 2.2). The intermediate and innermost domains have horizontal resolutions of 3 km and 1 km, respectively. All domains were configured with 31 vertical levels and a top level of 500 hPa. The boundaries for the two nested domains were adjusted to accommodate the complex terrain of the SFBA as represented by 30 arc-second terrain data in the WRF model. The North American Regional Reanalysis (NARR) dataset from 28 August 2003 at 0000 UTC was used for initial and boundary conditions and updated every 3 hours until a run completion time of 30 August 2003 at 0000 UTC.

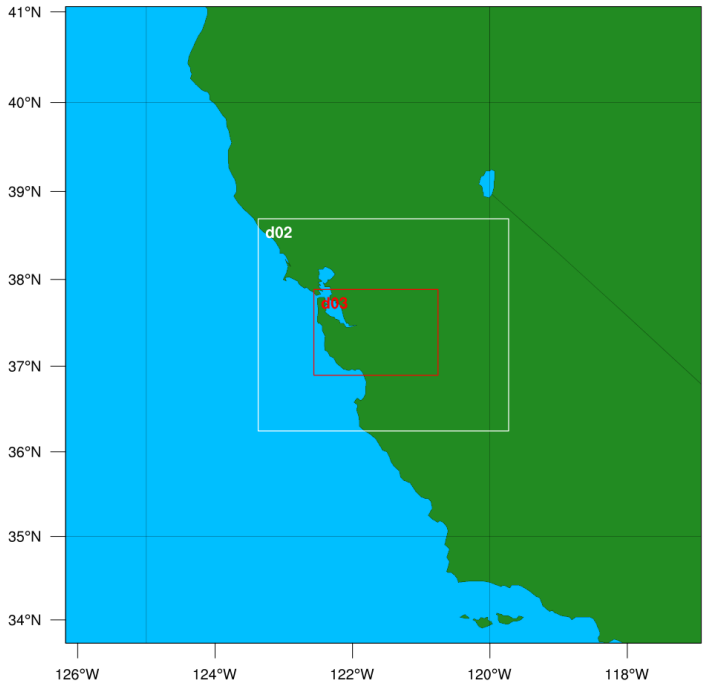

Fig. 2.2. Domain configuration used in WRF experiments.

3. Results

3.1 Climatology

A catalog of RAWS information and NDE count by site is presented in Table 1. Mt. Diablo and Mt. Wilson have the highest annually averaged number of events, with 49 and 50, respectively. Overall, the greatest number of annual NDEs occur in coastal California and above 2 km MSL in SN, suggesting broadly different mechanisms. In these areas, an excess of 25 events per year was found, while in OR and NC where driving mechanisms behind NDEs are less common, the annual frequency of events is much less (0 - 14). However, there is still a correlation between increasing NDE count and increasing elevation in all regions.

A more evident signal emerges when looking at NDEs between 1 May and 31 October in column 6 of Table 1. During the summertime, very little nocturnal drying is observed in OR, NC, and SN compared to SFBA, CC, and SC regions. SFBA is the only region where the number of summer NDEs outnumbers winter NDEs. In NC, Cooskie Mountain averages four NDEs during the fire season, which is 1-3 more than the others in that region. Similar amounts are found in SN, with a total of four at Mt. Tom and only 0-2 elsewhere. In OR, Sugarloaf and Bald Knob averaged only one NDE per summer. While SFBA, CC, and SC locations exhibit the greatest frequency of nocturnal drying during the fire season, there are more drastic differences between altitude and number of NDEs. In SFBA region, upper elevations during the summer months experience 5 -10 times the amount of NDEs as lower elevations, while a slightly more even distribution is seen in SC.

A spatial representation of NDEs between 1 May and 31 October shows that the greatest propensity for nocturnal drying is across elevated coastal terrain of California south of Pt. Reyes (Fig. 3.1.1). The uneven distribution of NDEs along this geographic stretch is most evident in SFBA and makes the case that elevation is as important as geographic location. SFBA and SC contain a diverse network of RAWS that allow for sampling at various altitudes and, in both of these regions, a general increase in NDEs is associated with an increase in elevation. The greatest number of summertime NDEs in the SFBA occur at the four uppermost RAWS in the region (MTD, RSP, MPC and BND) and are all at elevations above 710 m MSL, or the mean height of the marine layer during summertime. Counts at these respective stations of 37, 22, 14, and 15 NDEs correspond

to descending altitudes of 1173 m MSL, 933 m MSL, 792 m MSL, and 712 m MSL. The next closest site in this region is LSG with an average of four NDEs at elevation of 561 m MSL. Similar conditions exist in SC, where all RAWS above 900 m MSL averaged between 13 and16 NDEs per summer and the highest site (MTW) had the most with 27 MSL. At elevations below 900 m MSL, seasonal totals were five or less.

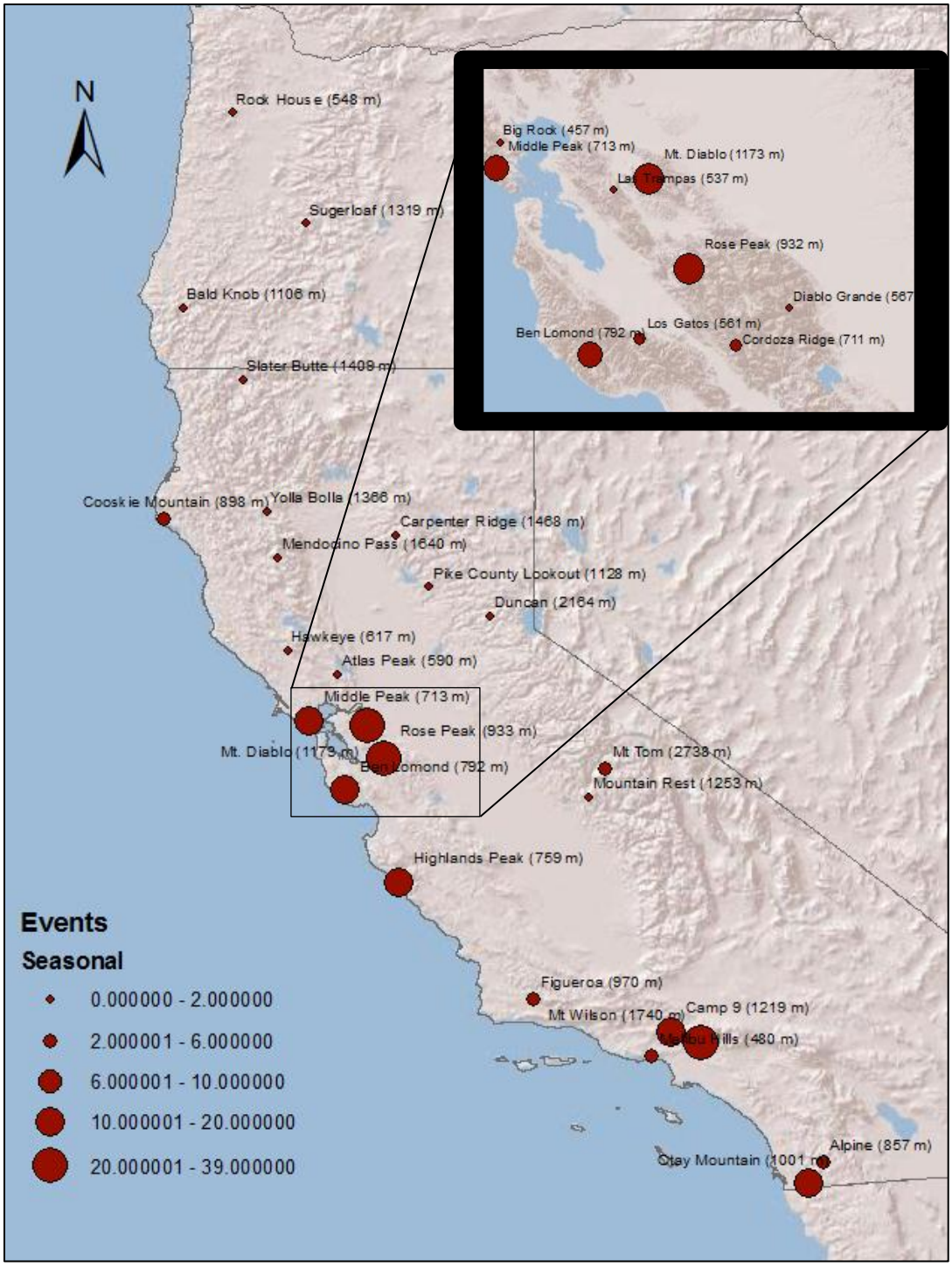

Fig. 3.1.1. Spatial extent and average number of NDEs between 1 May and 31 October 2000-2014. Larger circles represent greater amounts of events (see key).

Based on the greater frequency and summertime tendency of NDEs in the SFBA region, further analyses of seasonal and daily variability, as well as pertinent meteorological and fuel variables from MTD, RSP, MPC and BND were conducted. A very clear pattern emerges in both seasonal and diurnal occurrences of extremely dry air when looking at times when RH is below 9.5% and DP is less than or equal to -10.0º C. The overwhelming majority of extreme drying takes place between June and September at all four stations and the months of July and August account for approximately 40% of all occurrences (Fig. 3.1.2). A much less pronounced spike occurs during the winter months of December and January, most likely due to cold frontal passages. The two locations closest to the coast show more of a seasonal delay, with a lower relative frequency of occurrence during June at MDC and BND than MTD and RSP, and vice versa during September. All four stations also exhibit a steep decline during October.

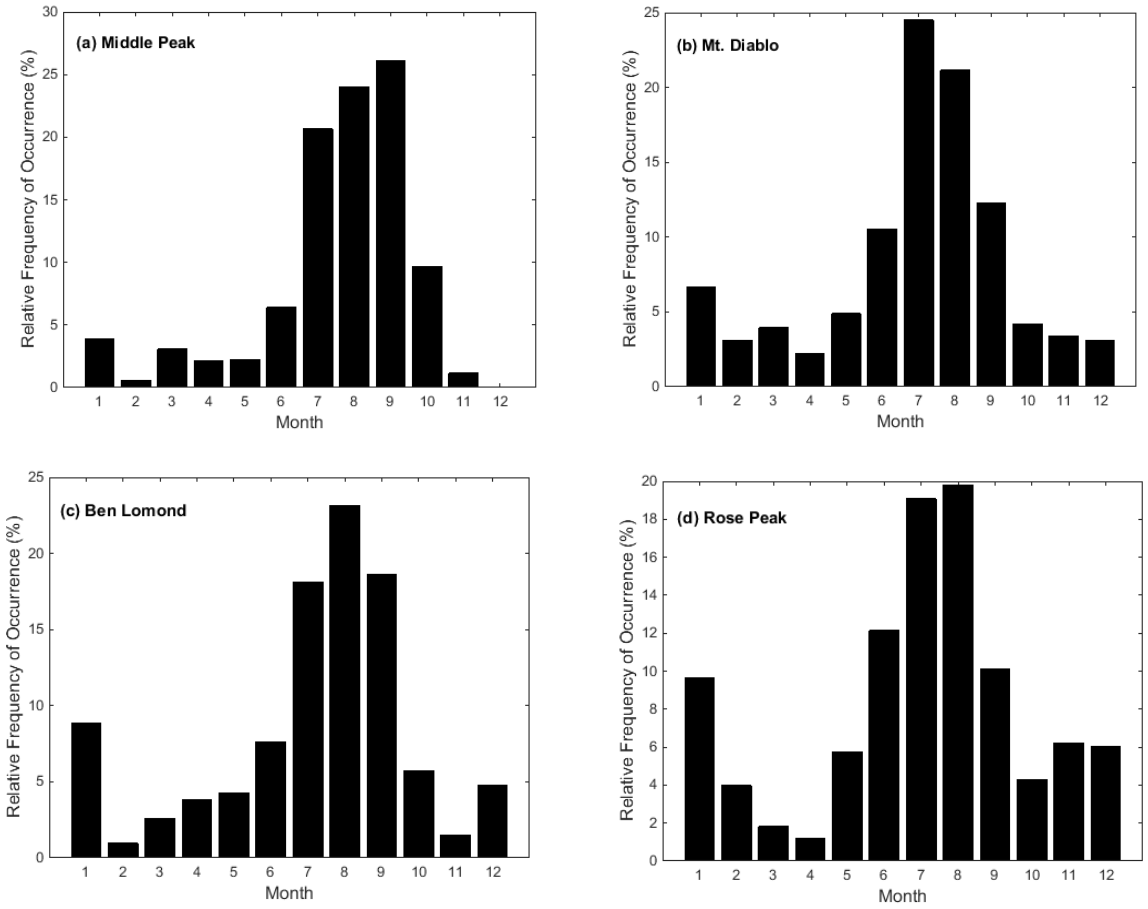

Fig. 3.1.2. Relative frequency of occurrence (%) by month when RH < 9.5% and DP < = -10 °C for Middle Peak (a), Mt. Diablo (b), Ben Lomond (c), and Rose Peak (d) between 2000-2014.

Another distinct pattern can be seen in Fig. 3.1.3, which shows the time of day that such extremely dry air occurs between 1 May and 31 October. A U-shaped distribution of occurrence is evident at all stations that show a maximum near midnight and minimum near 1400 PDT. At all locations, more than 75% of extreme drying takes place between 2000 and 0800 PDT and less than 10% between 1200 and 1600 PDT. The observed cycle in drying events is out of phase with the diurnal temperature cycle (Whiteman, 2000).

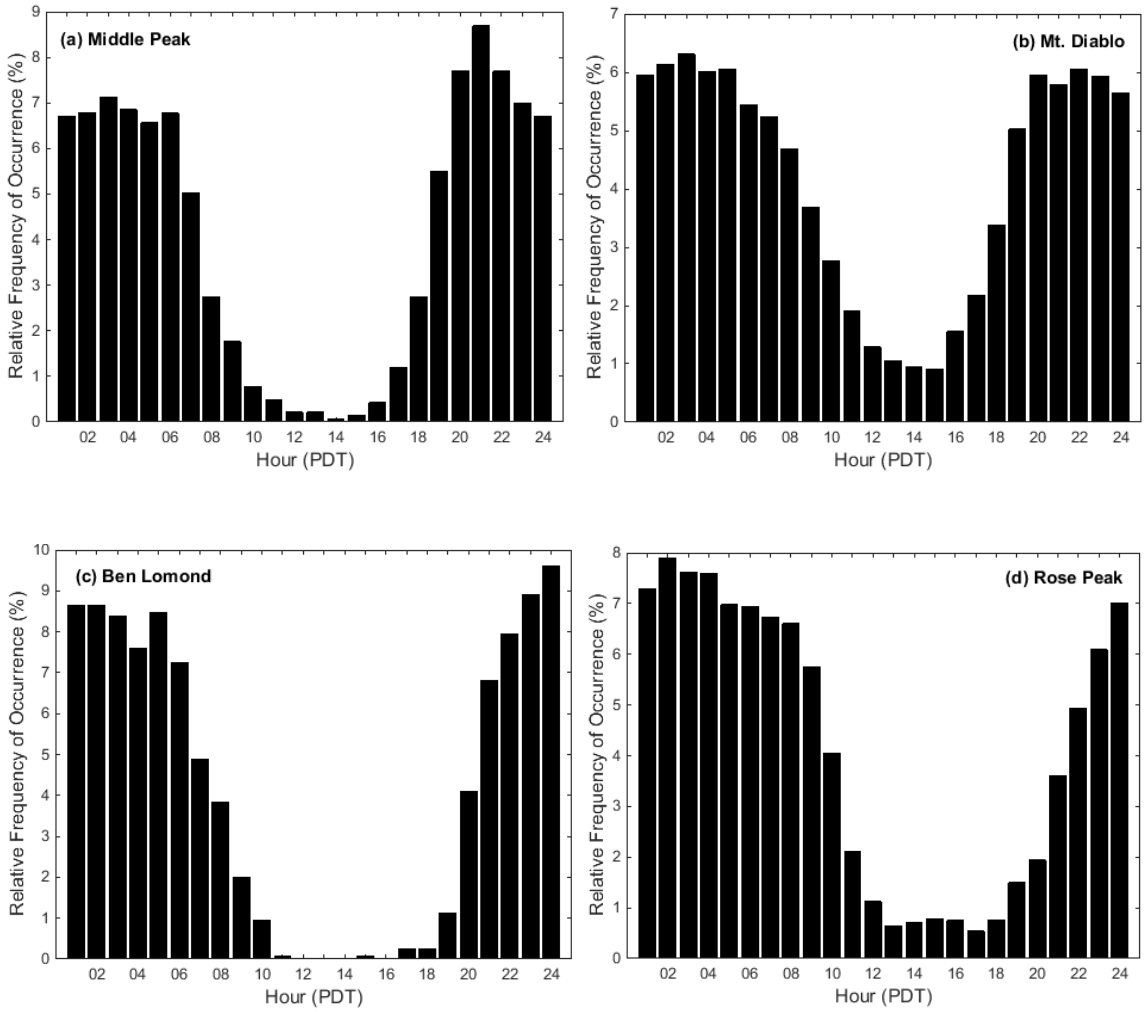

Fig. 3.1.3. Same as 3.1.2 except for relative frequency of occurrence (%) by hour (PDT) between 1 May and 31 October.

Wind roses are presented in Fig. 3.1.4 from times that satisfy the same criteria of simultaneous single digit RH and DP below or equal to -10º C during 1 May – 31 Oct. A consistent lack of an easterly wind component is apparent at each station. The two coastal locations, MDC (Fig. 3.1.4a) and BND (Fig. 3.1.4c) have more of a northwesterly direction, which corresponds to the prevailing summertime winds along the coast

(Neiburger, 1961). Wind speeds of 5 -10 m s^{-1} at MDC are much less than those at BND (< 5 m s^{-1}). Rose Peak (Fig. 3.1.4d) has the greatest directional variability and lowest wind speeds of all four stations. This could be partially due to the fact that it is the most sheltered site of the four sites; located in the upper slopes of an approximate north-south oriented ridge and perpendicular to a prevailing westerly flow. Conversely, the most exposed and elevated site (MTD) claims the strongest winds with prevailing directions between 135º and 305º (Fig. 3.1.4 b). Wind speeds in excess of 10 m s^{-1} are common at MTD and maximum speeds up to 22 m s^{-1} favor the southwesterly sector.

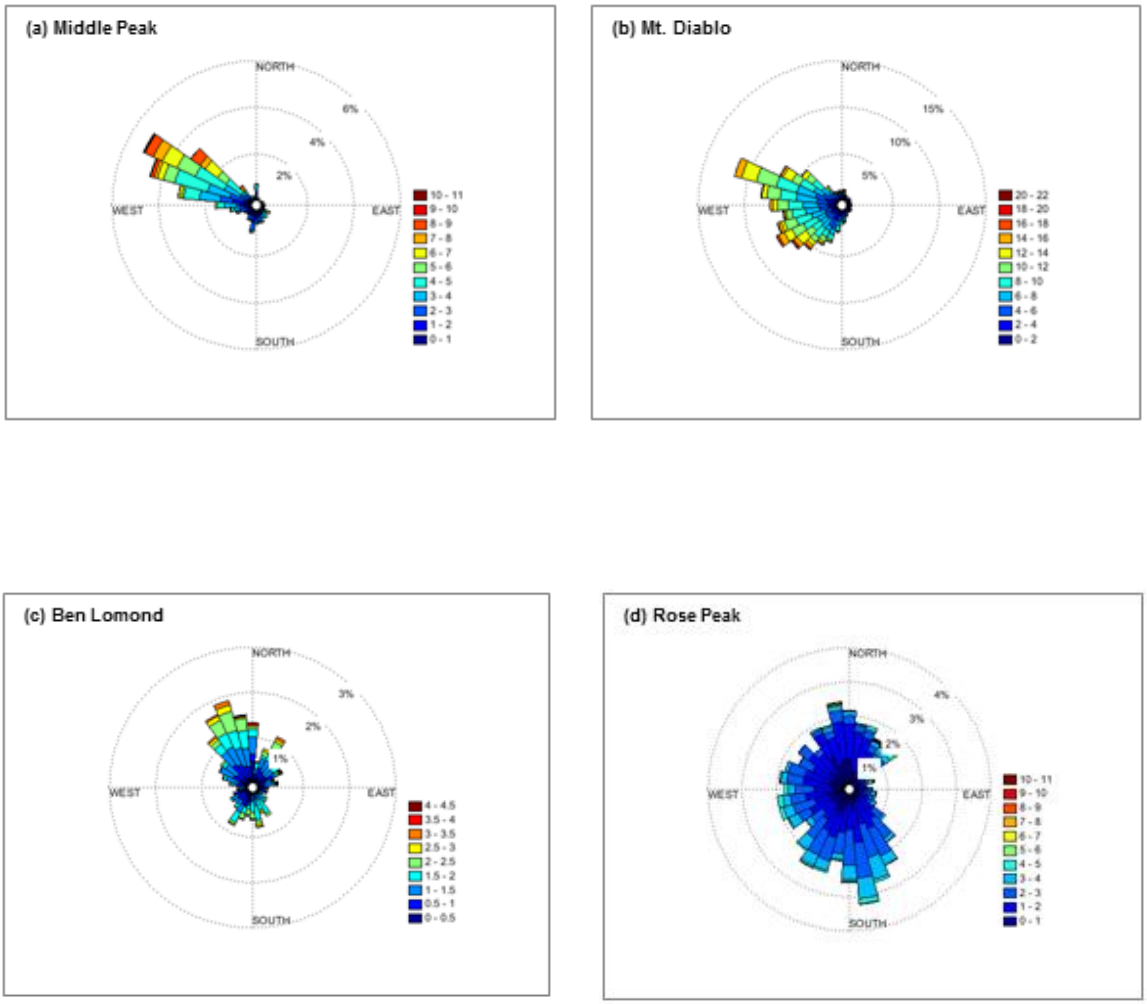

Fig. 3.1.4. Wind rose plots of wind speed (m s^{-1}) and direction for Middle Peak (a), Mt. Diablo (b), Ben Lomond (c), and Rose Peak (d) during NDEs from 1 May – 31 Oct 2000-2014. Circles represent relative frequency of occurrence.

Nocturnal drying events are outliers relative to most climatological statistics and have values well outside of 25th and 75th percentiles. Figures (3.1.5-8) display pertinent statistics of meteorological variables from MTD, RSP, MPC, BND, and LTR. Mean, 25th percentiles, 75th percentiles, maximum values, and minimum values at all five stations during summertime are shown. Also plotted for each station are average and extreme

values during NDEs with a general onshore wind direction between 150º and 360º. Mean summertime temperatures range between 15 and 20ºC, with 25th and 75th percentiles within 3-6ºC (Fig. 3.1.5a). During NDEs, temperatures are higher than average, but still generally within upper percentile bounds, and extreme values lie between 30 and 35ºC. Greater discrepancies are found between normal summertime moisture characteristics and times of extreme nocturnal drying associated with onshore flow. Figure 3.1.5b reveals an overall downward trend of mean RH and associated percentile brackets with altitude. At the lowest elevation of 537 m MSL, LTR has a mean summertime RH of 52%, while MTD averages just below 30% at an elevation of 1173 m MSL. More important is the departure from normal during NDEs when RH values average around 5% and bottom out at 1% at all stations.

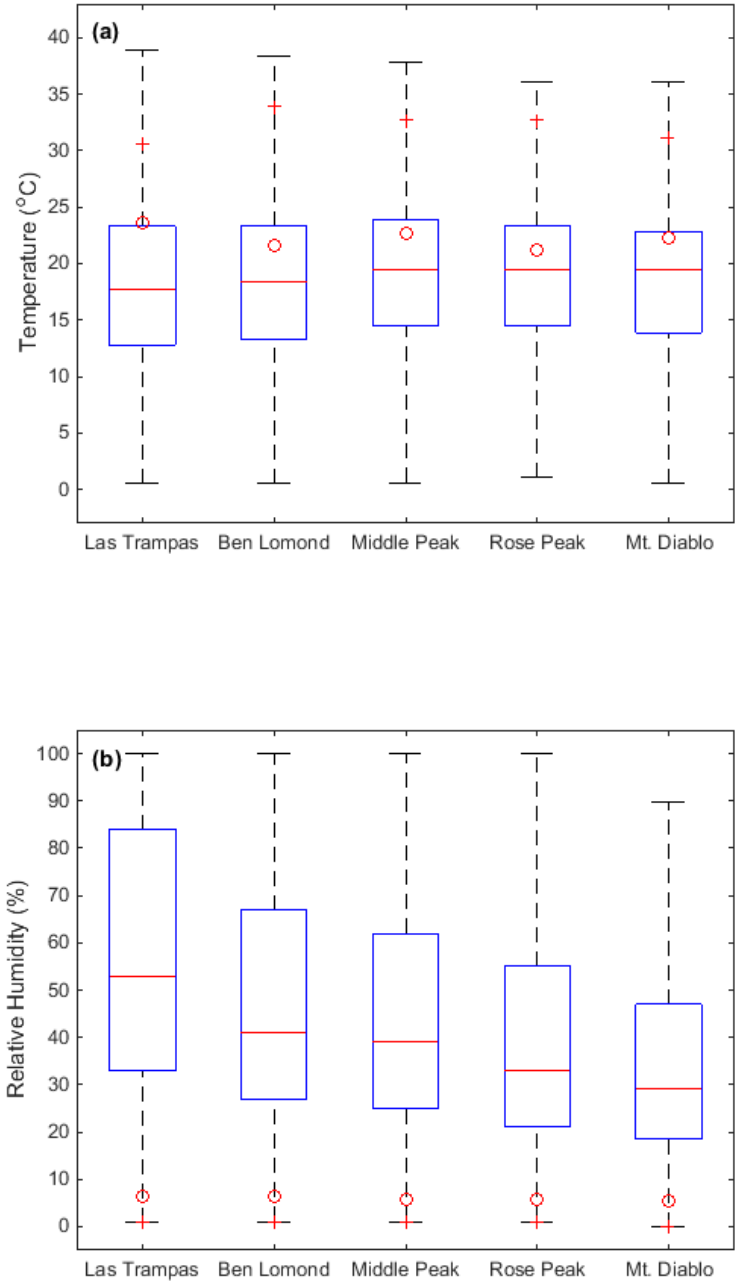

Fig. 3.1.5. Surface temperature and moisture variables from Las Trampas, Ben Lomond, Middle Peak, Rose Peak, and Mt. Diablo RAWS during NDEs. The red line represents mean summertime (1 May – 31 Oct) values and edges of the blue box represent 25th and 75th percentiles. Black ticks represent min and max summertime values. Red circles represent average values during NDEs and red crosses are extreme (min or max) values observed during NDEs.

The lack of moisture, not temperature, is responsible for such low RH during drying as seen in dew point temperatures and vapor pressure (Fig. 3.1.6a,b). Significant departures from summertime dew point temperature means on the order of 15-20ºC are present during NDEs (Fig. 3.1.6a). Normal values between 5 and 10ºC drop closer to -20ºC during NDEs and extreme values below -35ºC are common for all sites. Vapor pressure (Fig. 3.1.6b) exhibits similar characteristics as RH, with values decreasing with elevation and anomalously low values near zero during onshore dry periods.

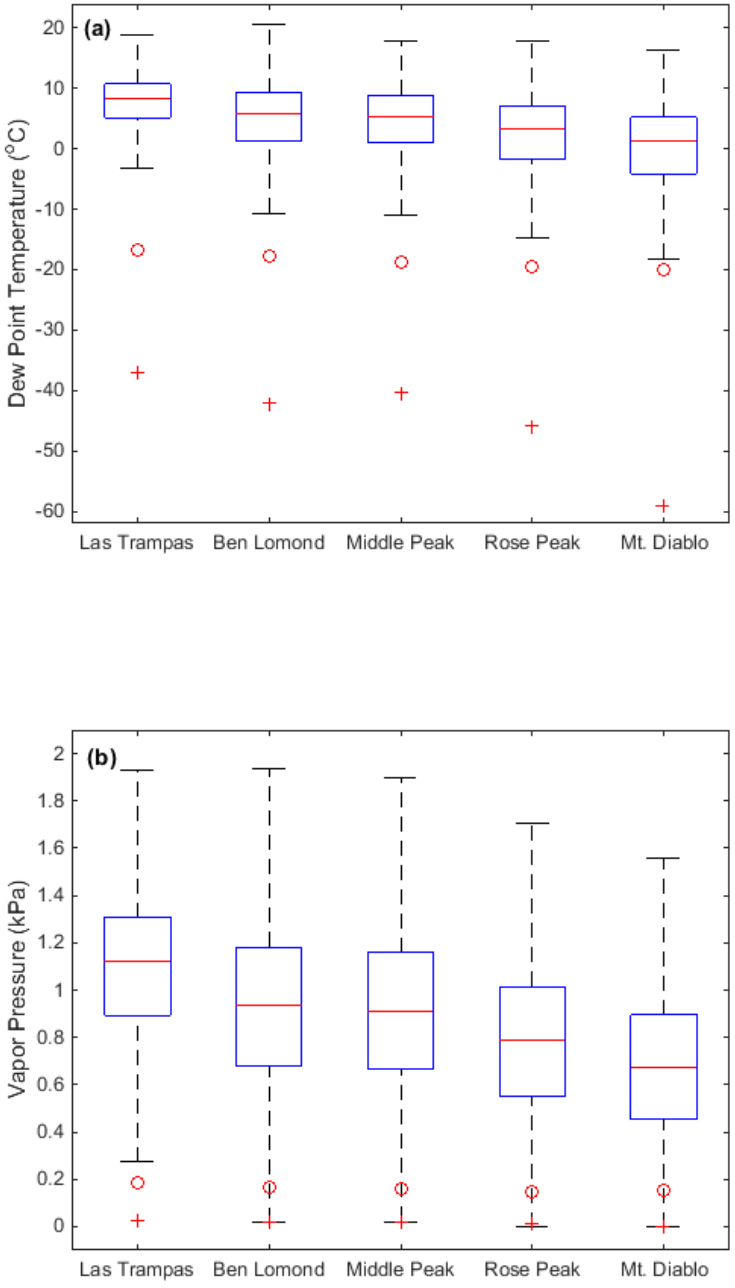

Fig. 3.1.6. Same as 3.1.5 except for dew point temperature (a) and vapor pressure (b).

Measurements of fuel temperature (Fig. 3.1.7a) and moisture (Fig. 3.1.7b) display characteristics similar to those found in the atmosphere. Mean fuel temperatures do not show much variance between normal summertime conditions and extreme drying, falling somewhere between 17 and 23º C, but values are elevated during times of NDEs. However, fuel moistures show a more significant departure from normal during drying, with most values below the 25th percentile and less than 5%.

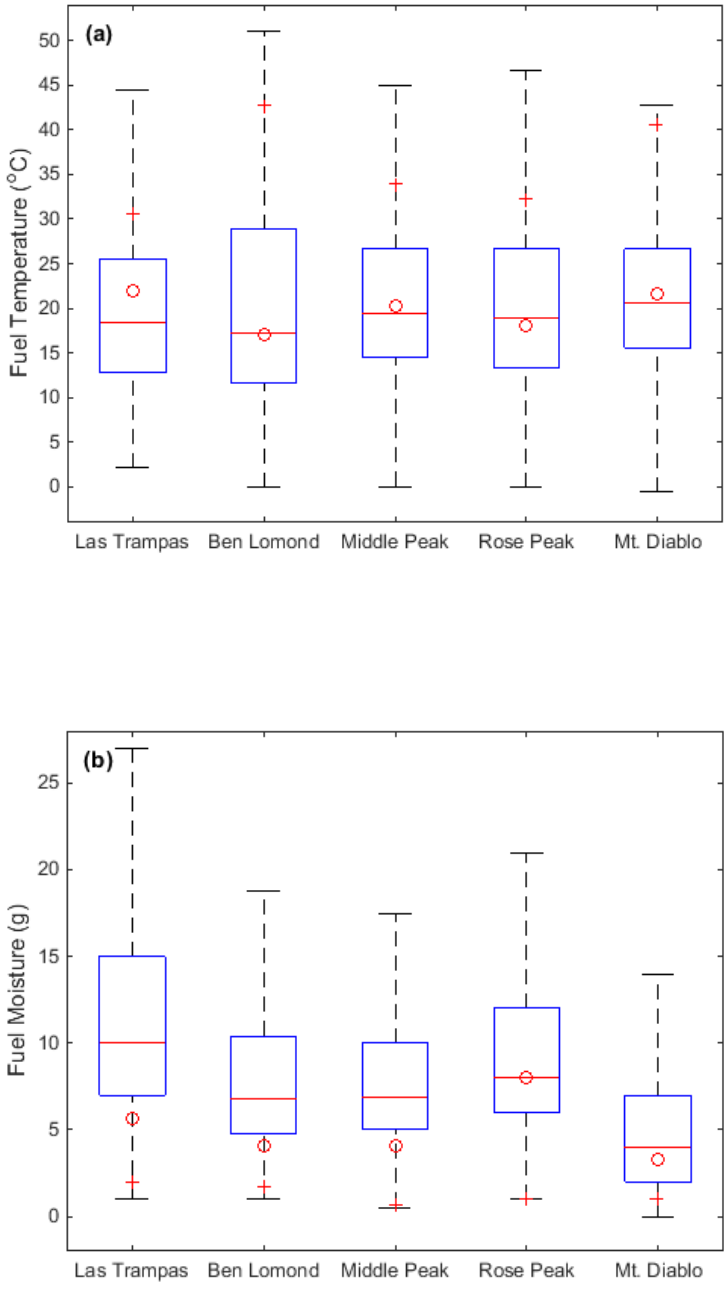

Fig. 3.1.7. Same as 3.1.6 except for fuel temperature (a) and fuel moisture (b).

Wind speeds offer less significant results and vary widely between each station (Fig. 3.1.8). Ben Lomond and RSP experience the lightest winds regardless of dry or normal conditions and generally remain below 5 m s^{-1}. This could partially be due to their more sheltered location, although the remaining three and more exposed sites only have average wind speeds closer to 5 m s^{-1}. MTD is the exception, with mean wind speeds of 5 –10 m s^{-1} and maximum speeds near 20 m s^{-1}.

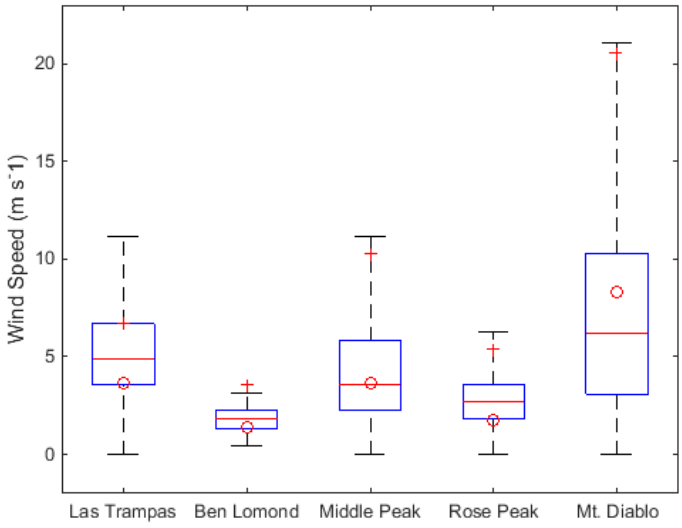

Fig. 3.1.8. Same as in 3.1.7 except for wind speed.

While the atmospheric conditions during NDEs can be similar regardless of location, the frequency of occurrence and magnitude of drying is much greater in higher elevations. Sharples et al. (2012) compared extreme drying events in Australia based on dew point difference anomalies between low and high country locations. Similarly, this study compared dew point depression differences between MTD and LTR during NDEs at MTD. The results in Fig 3.1.9 show a drastic separation of extremely dry air and

relatively moist air within approximately 600 m. During NDEs at MTD, dew point depression differences between the stations are usually between 20 and 40ºC and can reach close to differences of 65ºC (Fig. 3.1.9). In fact, the relative frequency of occurrences with dew point depression differences above 50ºC is the same as those below 10ºC.

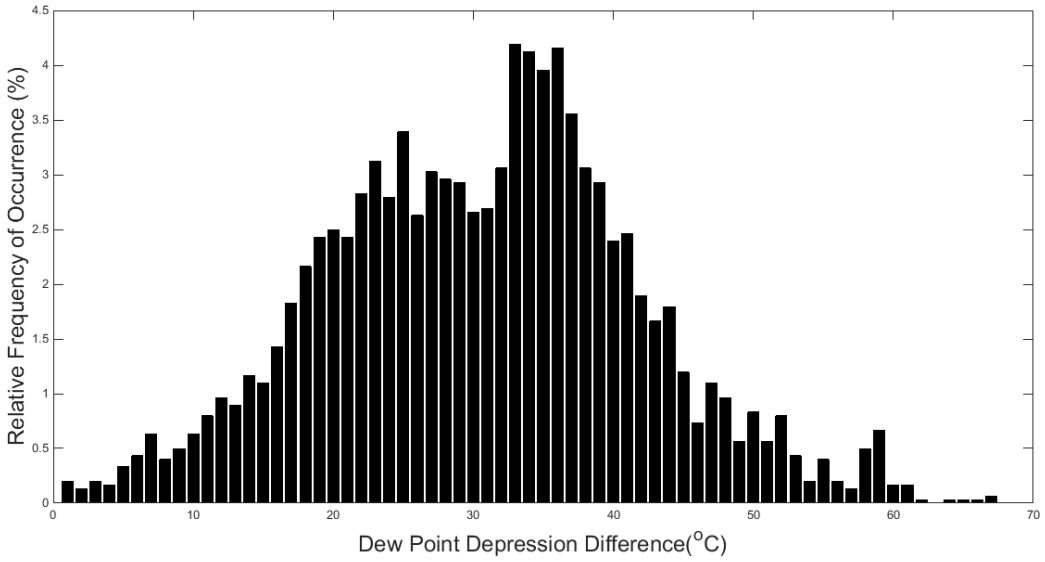

Fig. 3.1.9. Difference in dew point depressions between MTD and LTR during NDEs and representing an elevation difference of 636 m.

3.2 Composite Analysis

There have been cases of significant overnight drying occurring in multiple locations throughout the SFBA concurrently, with RH values and dew point temperatures reaching abnormally low levels. To further understand the circumstances under which more significant NDEs occur, large scale momentum, temperature, and moisture characteristics

of the atmosphere were investigated before, during, and after the most critical periods of nocturnal drying in the SFBA. Over the course of 11 summers between 2004 and 2014, 87 significant NDEs were identified for an average of eight per season. However, some years saw more than others, such as 2008 when 17 separate events occurred, while 2004-2006 only averaged around five.

a. Pressure levels

The evolution of such episodes is revealed by comparing specific features in the synoptic composites. The first composite analysis of interest is that of sea level pressure overlaid with 500 hPa heights (Fig. 3.2.1) and shows the synoptic progression surrounding significant nocturnal drying events in the SFBA. First, a short wave trough of low pressure can be seen in the 500 hPa height field amplifying as it approaches northern California in the 36 hours prior to event onset, while an upper-level ridge of high pressure simultaneously builds across the interior western U. S. (Fig.3.2.1a). The base of this trough is situated around 37°N and 145°W with an adjacent area of high pressure centered over northern Mexico. By T=0, the trough axis extends and shifts southeastward to 35°N and 137°W (Fig. 3.2.1d) as high pressure is displaced slightly eastward. By T+24, meridional flow at the 500 hPa level is at its greatest with a well-defined trough along the West Coast and a ridge of high pressure extending from the Four Corners region into southwestern Canada (Fig. 3.2.1f).

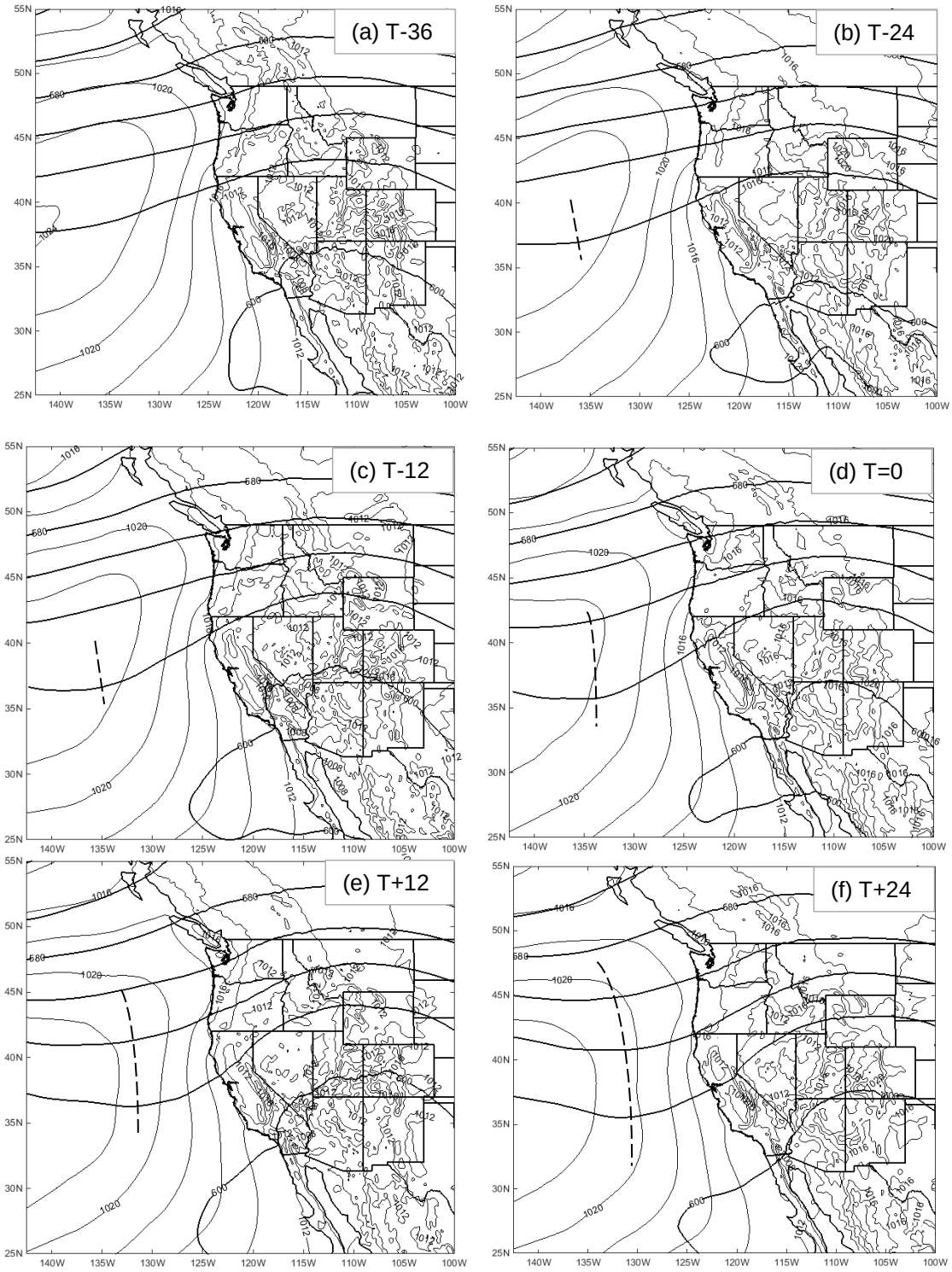

Fig. 3.2.1. Composites of 500 hPa heights (thick) and MSLP (thin) of 83 significant NDEs from the SFBA at 36 (a), 24 (b), 12 (c) hours prior to, during (d), and 12 (e) and 24 (f) hours after each event. Dashed line represents low pressure trough.

The opposite scenario is presented at the surface where an area of high pressure centered near 37°N and 145°W dominates the northeastern Pacific and a thermal low resides over the desert southwest (Fig. 3.2.1). At T-24, the northeastern periphery of a high pressure system extends into British Columbia, Washington, and Oregon representing a West Coast thermal trough associated with intense daytime heating as described by Brewer et al. (2012). As the upper-level trough of low pressure moves eastward, high pressure at the surface gradually weakens and shifts southward (Fig. 3.2.1a-f). The surface-based high pressure ridge extending into the Pacific Northwest, although still evident a day after the event (Fig. 3.2.1f), is less prominent and positioned farther south and west than at T-36. The surface area of low pressure over the southwestern U. S. can be attributed to strong diabatic heating and is a common summertime feature of the region (Whiteman 2000). Little change is observed during event progression of the thermal low, except for a slight eastward displacement. The juxtaposition of surface high pressure in the northeast Pacific and low pressure in the desert southwest creates a strong pressure gradient off the West Coast. The region of tightest pressure gradients also moves south from the northern California and southern Oregon coastal border to waters off the central California coast.

This synoptic set up allows for strong subsidence along the California coast drawing extremely dry air from upper to lower levels of the troposphere. The first ingredient for downward vertical motion and subsequent dry air is low-level divergence around the eastern periphery of the Pacific high. Divergence at the 925 hPa level (Fig. 3.2.2) shows an area of maximum divergence over western Oregon spreading off the northern

California coast to the south in a wedge-like shape between 120°W and 130°W. The strong divergence in this region is associated with a LLJ caused from pressure differences between high pressure to the west and low pressure to the east. Winds up to 11 m s^{-1} are found in the LLJ that correspond to areas of divergence. Areas of convergence around California can be attributed to the blocking effects of coastal terrain and surface friction (Burk 1996).

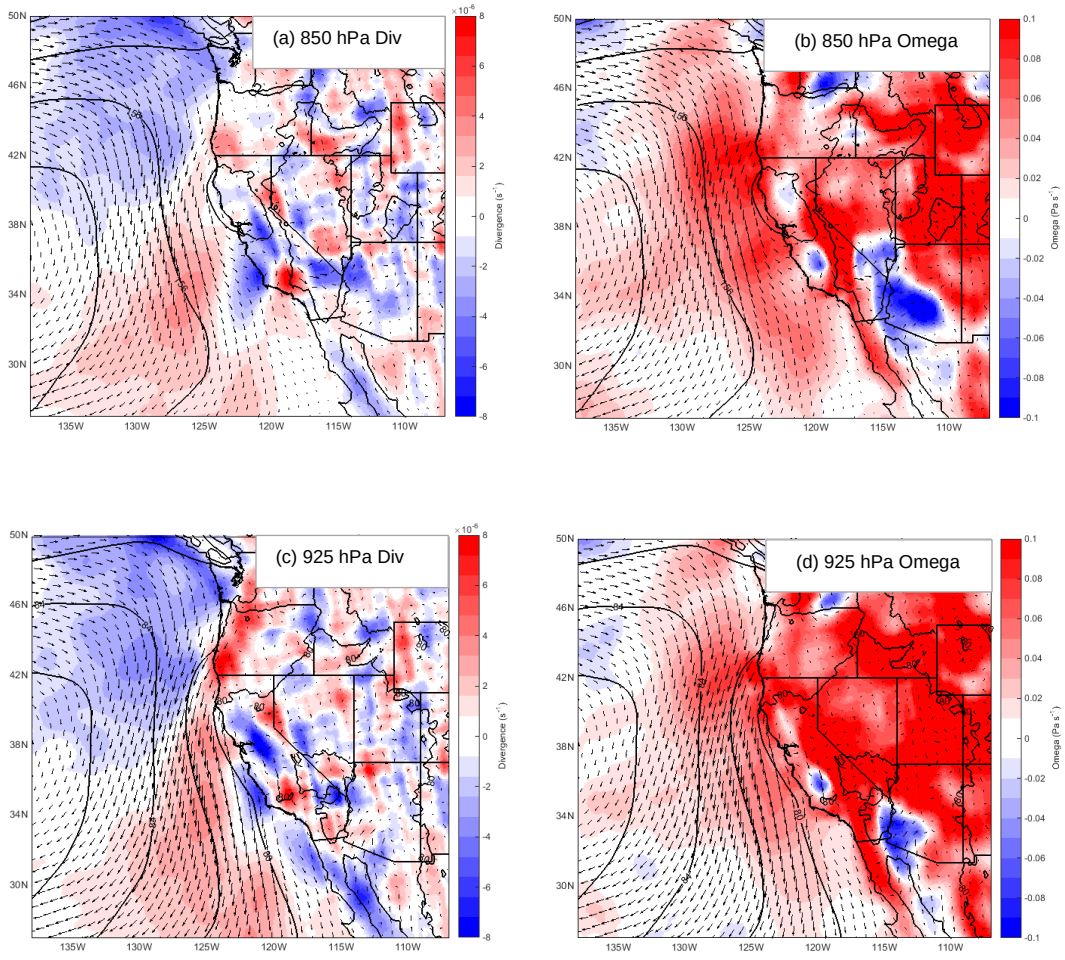

Fig. 3.2.2. Composites of 850 and 925 hPa heights (contours), winds (vectors), divergence (shaded) (left), and omega (shaded) (right) of 83 significant NDEs from the SFBA at T=0.

Similar features are found in 850 hPa analysis (Fig. 3.2.2) except for a wider area of non-divergence off the SFBA and a region of maximum divergence farther southwest than in at the 925 hPa level. The zone of non-divergence at 850 hPa corresponds to an area of maximum omega at the same level, signifying a broad region off subsidence in the lower troposphere off the California coast.

In the upper levels, an approaching upper-level trough provides another possible component for enhanced low-level subsidence. Figure 3.2.3 shows areas of divergence in the Pacific Northwest and convergence in California during NDEs associated with a trough over the northeastern Pacific and a ridge of high pressure over the Intermountain West. In the 500 and 700 hPa levels, an area of convergence is present over the SFBA, with negative omega at 500 hPa and positive omega off the California coast similar to 850 and 925 hPa levels.

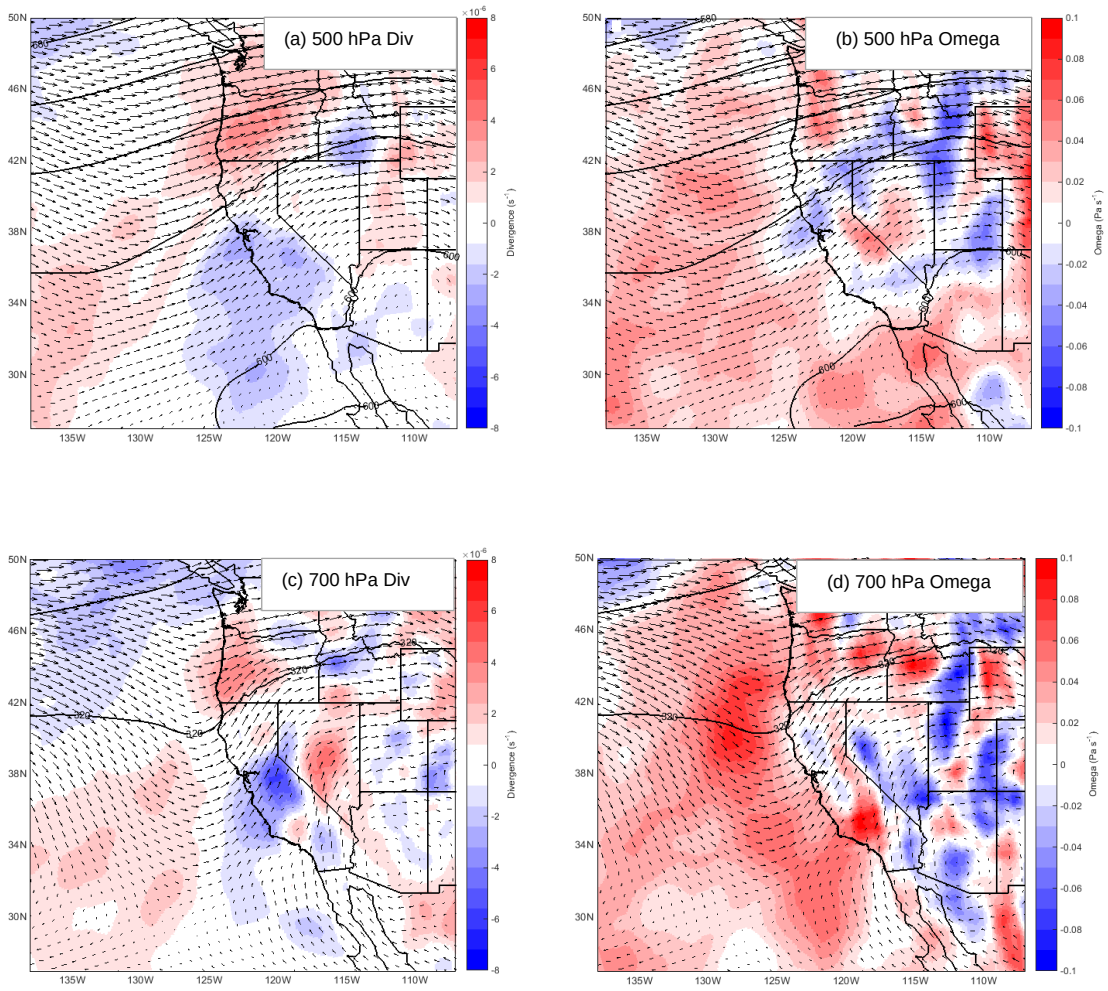

Fig. 3.2.3. Same as 3.2.2 except for 500 and 700 hPa.

A look at RH at various pressure levels shows evidence of very dry air associated with the subsidence-inducing factors of low level divergence and upper-level convergence (Fig. 3.2.4, 3.2.5). In the lower troposphere, the driest air is isolated to an area just off the central and southern California coast above the marine layer as well as parts of Nevada and southeastern California. Typical diurnal RH trends exist in the interior western U. S. with generally lower values during the daytime and higher values

overnight. While low RH across the interior can be attributed to warmer temperatures, the region of dry air along California (Fig. 3.2.4) corresponds to the area of divergence at the 925 and 850 hPa pressure levels and can be associated with subsidence. Figure 3.2.4 also displays a unique diurnal pattern where RH is higher across elevated terrain of SFBA and CC regions during the day and lowest at night when the dry air established along the coast pushes inland.

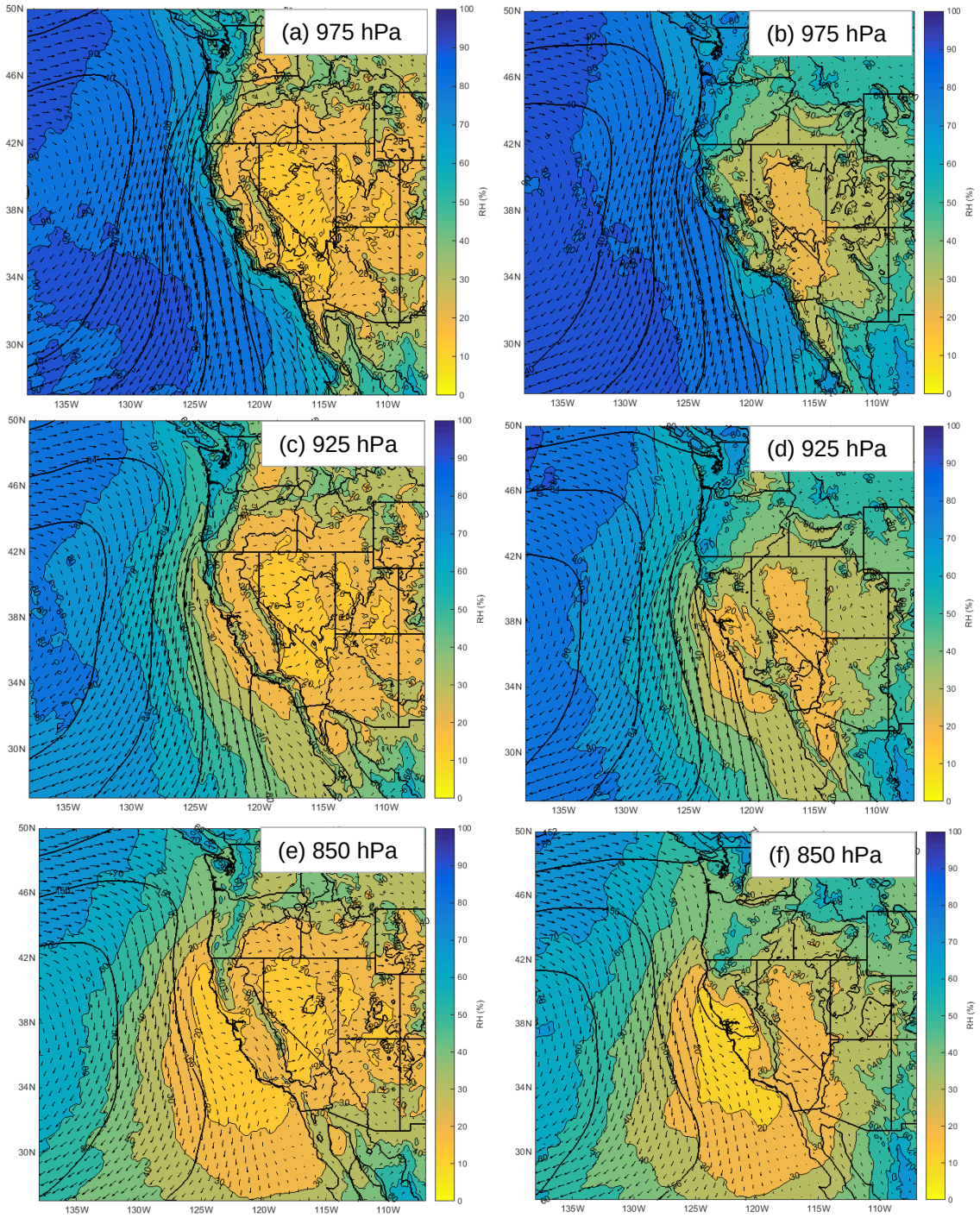

Fig. 3.2.4. Composites of 975, 925, and 850 hPa heights (contours), winds (vectors), and RH (shaded) of 83 significant NDEs from the SFBA at T-12 (left) and T=0 (right).

A much larger region of dry air is present off the California coast at 850 hPa that almost reaches the length of the entire state (Fig. 3.2.4e,f). Similar to 925 hPa RH, an inland intrusion occurs through the SFBA during nighttime hours and it should be no coincidence that the deepest inland extent of dry air occurs over the greater SFBA at T=0 (Fig. 3.2.4f) due to experimental design. During periods associated with significant NDEs, the driest air west of the Rocky Mountains at the 850 hPa level can be found off the California coast.

The 700 hPa analysis shows a pocket of lower RH over the southwestern portion of the domain that thins and separates into two lobes with one drifting over central California at T=0 (Fig. 3.2.5a,b). At the 500 hPa level, the spatial extent of lowest RH is greatest in the region south of 36°N and west of 120°W, with an elongated area of locally higher values extending northeastward (Fig. 3.2.5c,d). The tongue of driest air reaches the coast and inland portions of central California before and during the event.

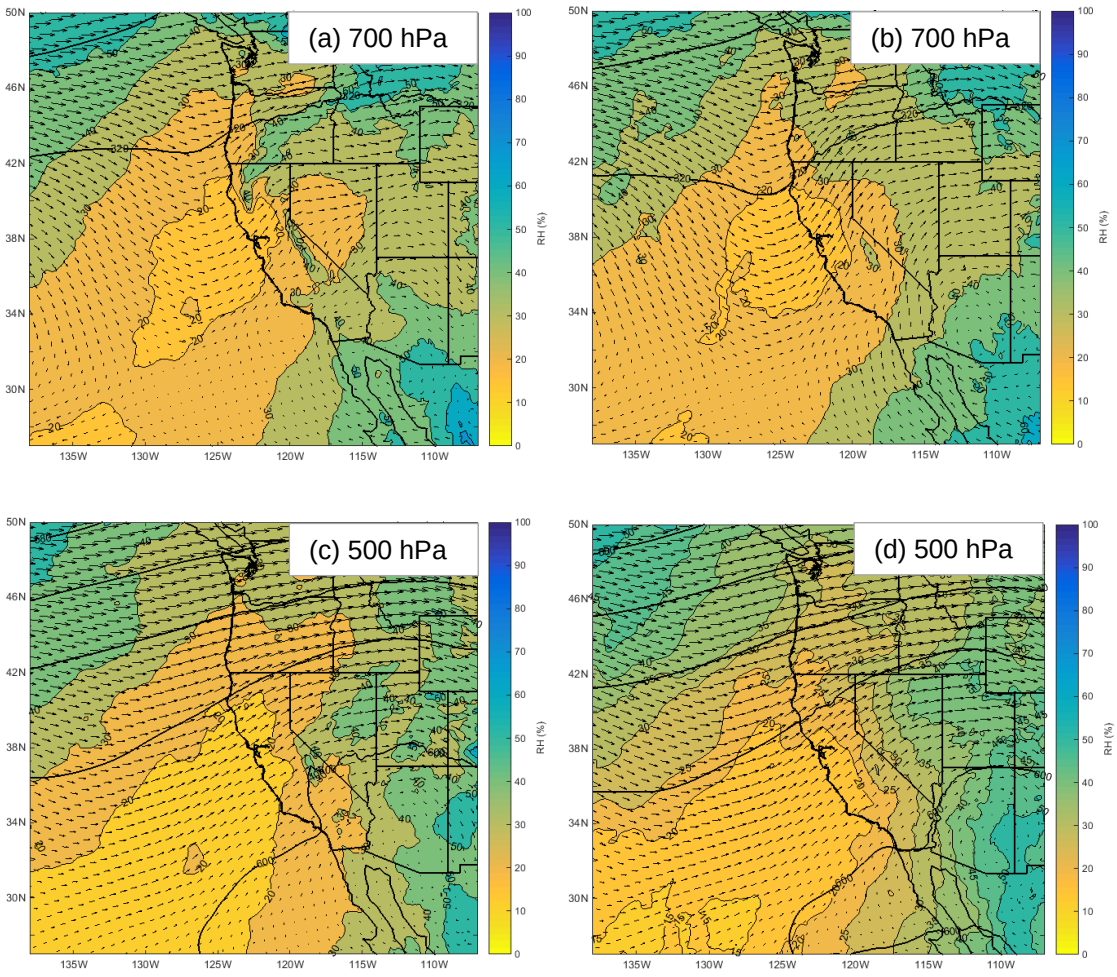

Fig. 3.2.5. Same as 3.2.4 except for 700 and 500 hPa.

Heights, winds, and temperatures at the 850 hPa pressure levels are presented in Fig. 3.2.6. A clear diurnal signal can be seen across the interior western U. S. as temperatures modify between day and night. Increased baroclinicity that arises between the warmer continent and cooler ocean enhances northerly geostrophic flow as marked by the LLJ offshore. Temperatures around 29°C can be seen in the Four Corners region, while the SFBA ranges from 19-21°C.

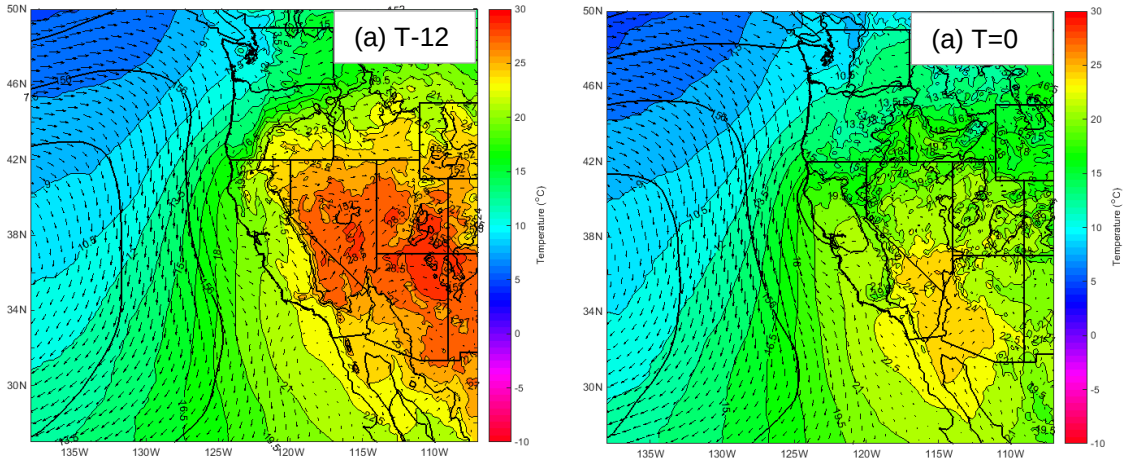

Fig. 3.2.6. . Composites of 850 hPa heights (contours), winds (vectors), and temperatures (shaded) of 83 significant NDEs from the SFBA at times T-12 (left) and T=0 (right).

In the afternoon following a NDE, warmer temperatures are observed in the central and northern Rockies as the ridge of high pressure strengthens over the western U. S. However, more noticeable is the decrease in temperatures after the event, especially near the coast and far northwestern California, where they lower 1-2°C the day after a significant NDE (Fig 3.2.7).

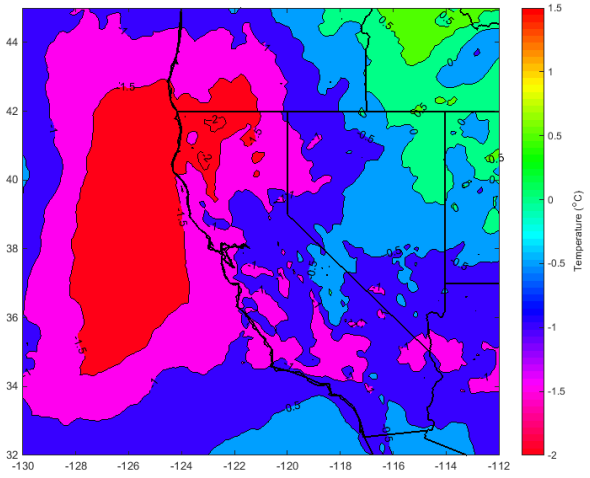

Fig. 3.2.7. 850 hPa temperature change between T-12 and T+12.

b. Upper air sounding

A pressure-averaged composite of 12Z KOAK soundings during 69 significant NDEs in the SFBA reveals an exaggerated Y-shaped temperature and dew point profile as a layer of extremely warm and dry air with dew point depressions greater than 40°C exists immediately above a shallow marine layer with dew point depressions less than 3°C (Fig. 3.3.1). Temperatures around 13°C at the surface reach 22°C at the inversion top (925 hPa), while conversely, dew point temperatures drop from 10 to -20°C through the inversion. Lapse rates in the inversion are on the order of 0.02°C m^{-1} for temperatures and -0.06°C m^{-1} for dew point temperatures. An overall onshore wind pattern is exhibited through the entire sounding. Westerly winds below 5 m s^{-1} near the surface turn to a south-southwesterly direction above the inversion top, and then transition to a more west-southwesterly direction above 500 hPa where speeds increase to between 10 and 20 m s^{-1}.

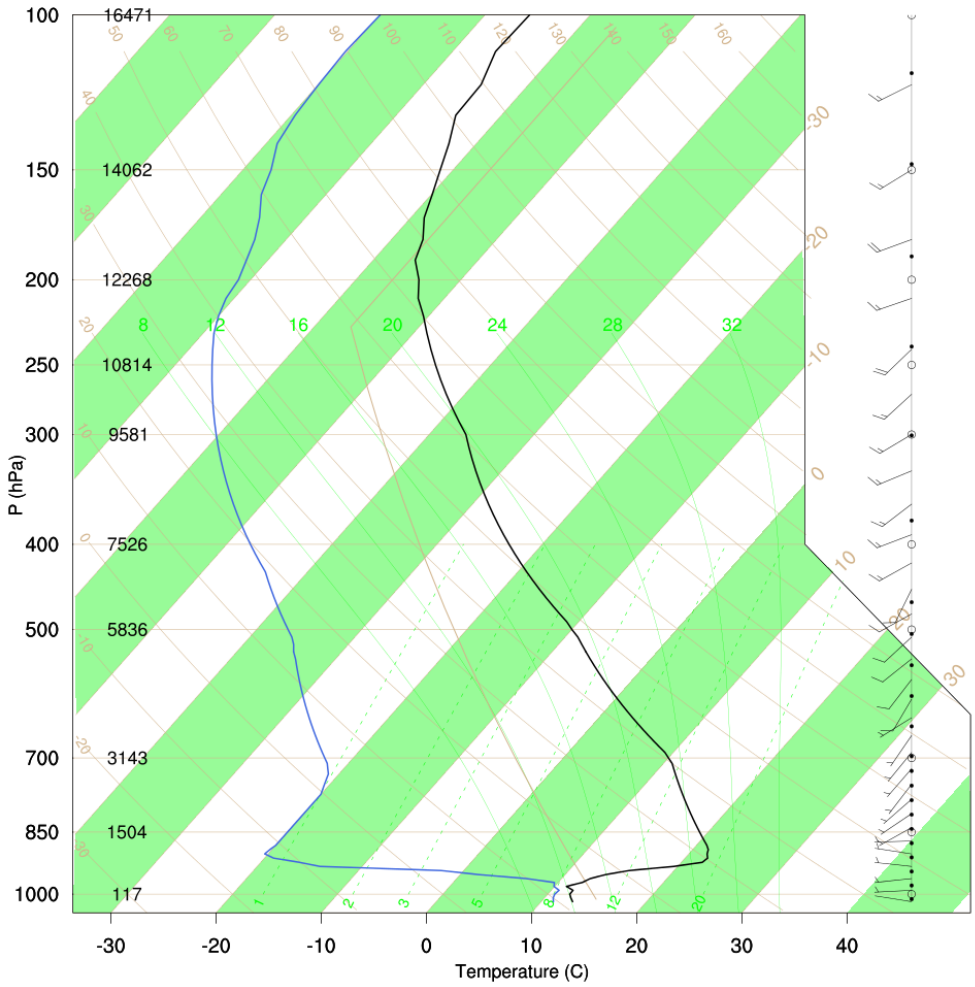

Fig. 3.3.1. Composite sounding from KOAK of temperature (black), dew point (blue) and wind barbs (m s^{-1}) during significant SFBA NDEs

The inversion base begins above the marine layer at 364 m MSL and continues to a height of 824 m MSL as indicated by the stable layer in the potential temperature profile (Fig. 3.3.2). The mixing ratio profile intersects the potential temperature profile near the middle of the inversion as values drop from 8 g kg^{-1} in the marine layer to 1.3 g kg^{-1} above the inversion. There is also a noticeable increase in wind speed from the surface to the top of the inversion. Westerly winds between 2 and 3 m s^{-1} in the marine layer below

the inversion base increase to speeds above 4 m s^{-1} in the nose of a LLJ situated in the few hundred meters surrounding the inversion top. Above the inversion, winds turn from a westerly to southwesterly direction but remain generally light at speeds between 3 and 6 m s^{-1}.

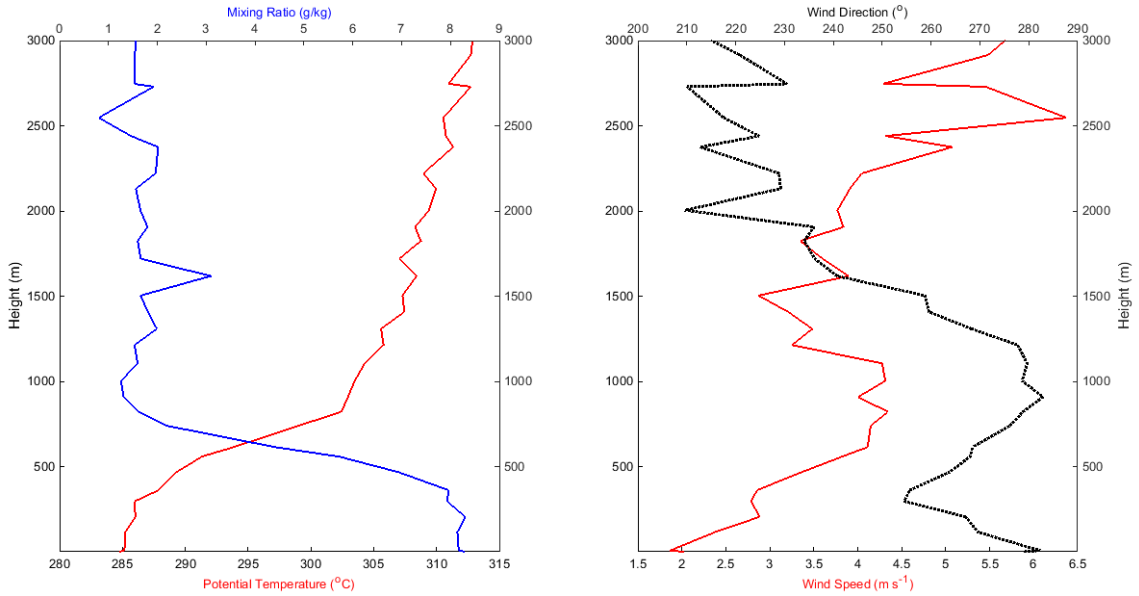

Fig. 3.3.2. Composite sounding from KOAK of potential temperature (red), mixing ratio (blue) (left) and wind speed (red) and wind direction (black) (right) during significant SFBA NDEs. axes

The northwest to southeast orientation of the California Coastal Ranges act as a barrier to southwesterly winds in the boundary layer and the prevailing flow must air must either be forced over the obstacle or proceed around it through coastal gaps. The Froude number, Fr, is the ratio of inertial to gravitational force that determines the behavior of a channeling flow with changing vertical boundaries (Fr = U/hN; U is the velocity of the layer, h is the height of the obstacle, and N is the Brunt-Väisälä Frequency). As demonstrated by Dorman et al. (1996), the shallow-layer Froude number

of the MABL can be calculated as $Fr = U/(gH\Delta\theta/\theta)^{1/2}$, where g is gravity, H is the mean inversion height, $\Delta\theta$ is the difference in potential temperature between the inversion base and top, and θ is the potential temperature at the inversion base. When the Froude number is less than 1, the layer is subcritical, air flows around the barrier, and gravity perturbation waves can propagate upstream. When the Froude number is greater than 1, the layer is supercritical, ascends the barrier, and gravity perturbation waves cannot propagate upstream.

Using values from the composite sounding ($U = 3$ m s^{-1}, $H = 560$ m, $\Delta\theta = 14.55$ K, $\theta = 285.42$ K) offers a low Froude number of 0.179, as would be expected given the weak flow and strong static stability of the layer. Therefore, the layer is subcritical and would flow around obstacles of equal or greater height. However, often times a Froude number closer to one is achieved in the SFBA when background winds are strong enough and inversion tops are equal to ridgelines. In this case, gravity wave formation and increased wind speeds are possible at crest levels and leeward mountain sides that would create an additional threat to fire behavior.

4. Devil Fire Case Study

Having established the climatological and synoptic context of NDEs, a specific case was examined in which sudden overnight drying exacerbated fire behavior and the subsequent overrunning of crews. Although this is one of the most dangerous cases encountered by firefighters, local agencies have long recognized the potential for more active fire growth in the higher coastal topography of the SFBA and central California during overnight hours.

4.1 Overview

Late at night on 26 August 2003, an intense convective outbreak resulted in thunderstorms over the Diablo Range and 81 lightning strikes between 2200 and 0000 PDT as determined by the National Lightning Detection Network (Walbrun 2004). By the next day, a group of 23 fires collectively known as the Santa Clara Complex would go on to burn 31,000 acres. Nearly 48 hours after the first lightning strike, the largest emergency fire shelter deployment in California history and second largest in U. S. history took place when a fire overran crews battling the Devil Fire in a remote and rugged portion of the northern Diablo Range (Fig. 4.1.1)

Fig. 4.1.1. MODIS Satellite imagery from 27 August 2003. A group of 23 fires collectively known as the Santa Clara Complex can be seen burning in red perimeters throughout the Diablo Range.

According to a California Department of Forestry and Fire Protection Review (CA-SCU-003581, 2003), at approximately 0115 PDT on 29 August 2003, two California Department of Forestry (CDF) overhead personnel, two dozer operators, and 51 CDF Inmate Conservation Camp Fire Crew firefighters become entrapped while performing a holding operation along a ridge at 1100 m MSL near Eylar Mountain. The crew was reassigned to the fire earlier in the evening and made their way up a ridge to assist in a planned firing operation that would aid in containment by eliminating fuels and establishing a perimeter ahead of the fire front. The main fire was burning in a canyon below and the fire behavior that evening was described as moderate to low intensity while making short uphill runs. The firing operation began at approximately 2235 PDT and was terminated shortly after midnight when crews could not get fire to ignite.

At approximately the same time, the main fire from below became active as RH lowered and winds turned from a westerly to a north-northwesterly direction, aligning with the direction of the canyon. Flame lengths of 9-15 m were observed until the fire reached brush fuel in slopes of 70–80%, and then flame lengths increased to 30 m. Rapid upslope runs, some in excess of 300 m over a 2-3 minute period, and spot fires over 400 m ahead of the fire were also observed. As the fire spread upslope toward the crew and it was realized they could not make it to a designated safety zone, a firing operation was carried out surrounding the perimeter of the shelter deployment site in an area of lighter fuels. The deployment lasted for 10-15 minutes. During the entrapment, 53 fire shelters were successfully deployed while the two dozer operators took refuge in their

enclosed cabs. The only injuries were second degree burns less than 2 cm in diameter experienced by two CDF employees and one inmate.

4.2 Observed Meteorological Conditions

A weather summary from the CDF Review (CA-SCU-003581) described a weak, small–scale trough of low pressure moving across northern California, increasing the inland extent of the marine layer with a depth of approximately 760 m. Relative humidity values above the marine layer that evening were measured in the 25-30% range at an elevation of 914 m MSL and dropped between 14-20% after midnight. At 0100 PDT, just before the fire shelter deployment, RH values of 6% were documented near the deployment site. Wind speeds were estimated to be 4 m s^{-1}. The nearby Rose Peak RAWS station, also reported an abrupt drop in RH accompanying a shift in winds from a westerly to northerly direction (Fig. 4.1.2, 4.1.3) around midnight on 29 August. After midnight, RH decreased to 5-10% and did not recover until after sunrise.

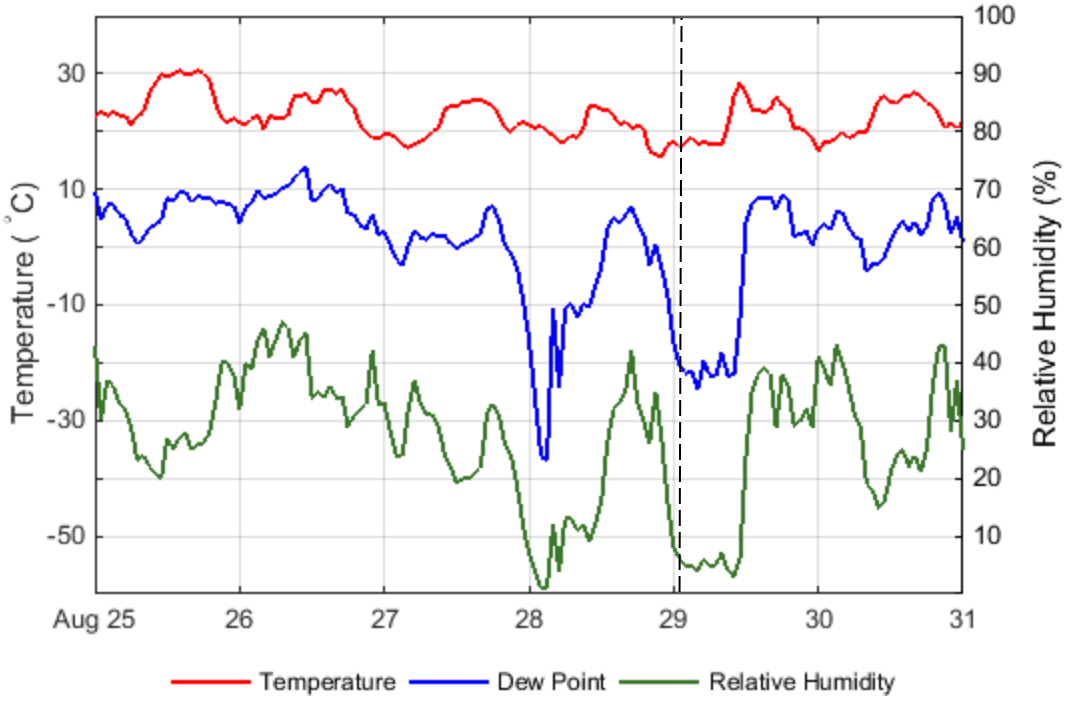

Fig. 4.1.2. Time series of temperature and moisture variables from RSP during the days surrounding the Devil Fire shelter deployment on 29 August at 0115 PDT (dashed line).

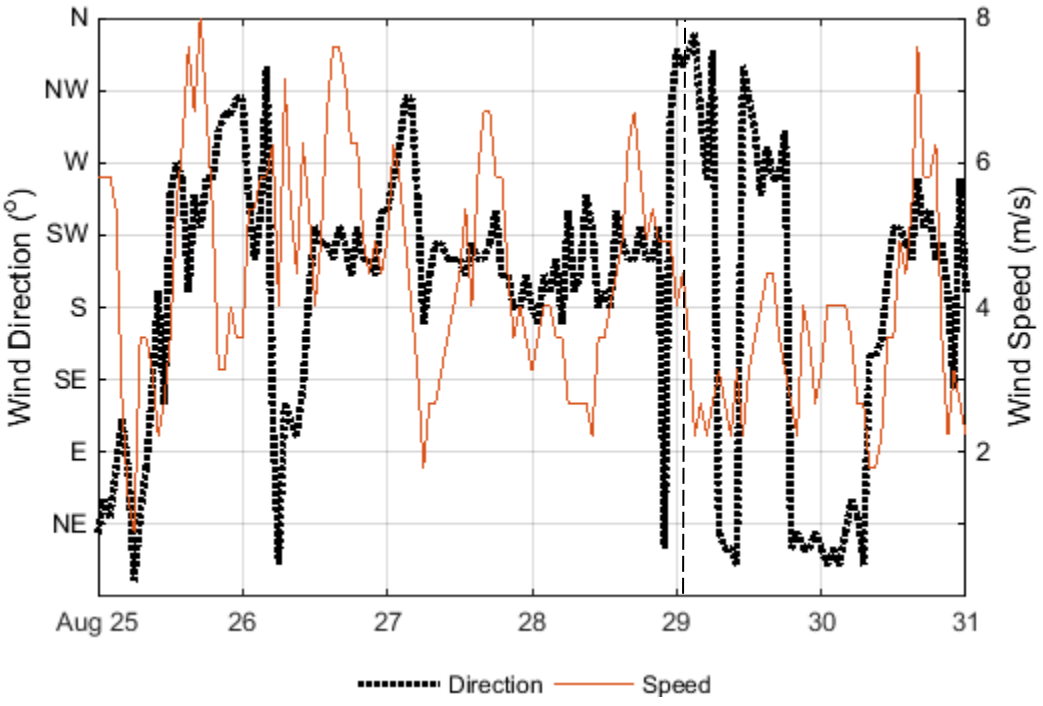

Fig. 4.1.3. Same as 4.1.2 except for wind speed and direction.

There are several features of note that stand out in Figure 4.1.2. First, much lower RH values were recorded during the night prior to the Devil Fire overrunning, with an equally abrupt drop during the same time. Whether this had any effect on fire activity in the area at the time is unknown. Second, decreases in RH correspond closer to dew point temperatures than air temperatures. Therefore, moisture deficiencies are more important than temperatures during this NDE, and as demonstrated from the climatology, in NDEs in general. Finally, the diurnal patterns of temperature and dew point are generally in phase with each other, which is the opposite of typical diurnal cycles and unique to RAWS in the upper elevations of the SFBA. Dew point temperature trends coincide with air temperature trends, reaching maximum values during the daytime and minimum values overnight; to varying degrees.

A general diurnal pattern can also be discerned from wind speed and direction in the days surrounding the Devil Fire incident (Fig. 4.1.3). In the days leading up to 29 August, wind speeds peak at RSP around 3.5 m s^{-1} in the late afternoon and reach a minimum overnight through the following morning. Wind direction is southwesterly in the afternoon when wind speeds are at their greatest. Just before 0000 PDT, a transition from westerly to northerly wind coincides with abruptly declining dew point temperatures and RH values. Wind speeds decrease from 2.5 m s^{-1} to less than 1 m s^{-1} during the onset of dry air.

The event persisted through 1035 PDT but within two hours, a rapid humidity recovery back to the 30-40% range was observed, even though winds remained out of the north until later in the afternoon. Immediately before the transition, there is a slight

uptick in wind speed, decrease in dew point depression, and increase in RH values; attributes of a weak marine layer or inversion top. That same signal can be seen a few hours earlier and, to a greater extent, in the evening prior. The maximum temperature from RSP on 28 August was 24.4°C. During the NDE, temperatures varied from 18.9°C to 17.2°C before increasing after sunrise.

The measurements from RSP match well to the 0500 PDT upper air sounding from KOAK (Fig. 4.1.4) from 29 August. Here, a sharp inversion is present near 925 hPa (785 m) that separates dew point depressions less than 5°C in the marine layer from dew point depressions greater than 20°C above the inversion. Veering winds are present below the inversion and backing winds above; both at speeds below 5 m s^{-1}. GOES visible satellite imagery (Fig. 4.1.5) confirms fingers of stratus intruding into coastal valleys from a main source region blanketing the coast and extending hundreds of kilometers over the northeastern Pacific.

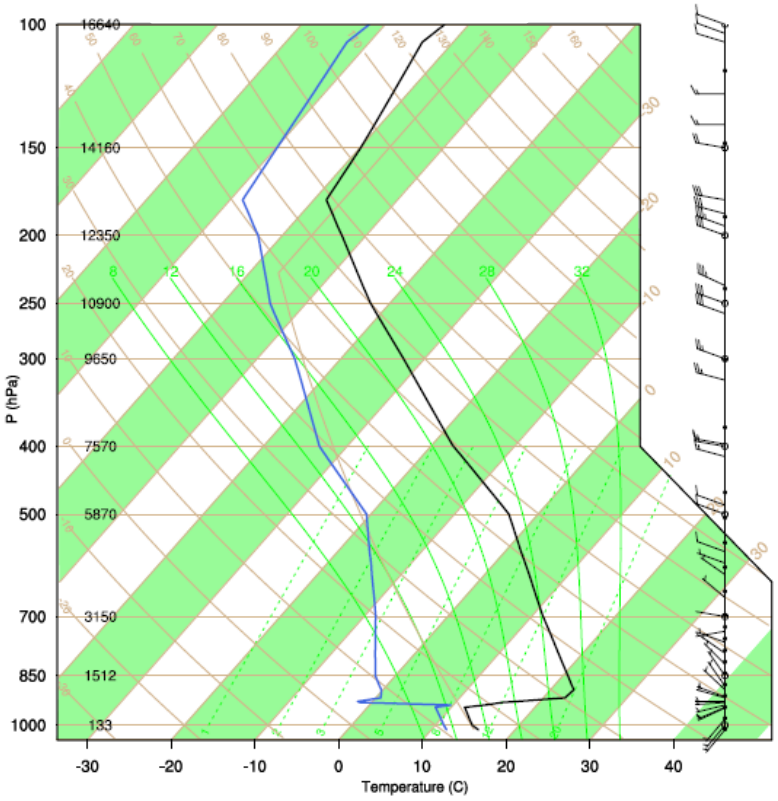

Fig. 4.1.4. KOAK upper air sounding from 29 August 2003 (0500 PDT) of temperature (black), dew point (blue) and wind barbs (m s^{-1}).

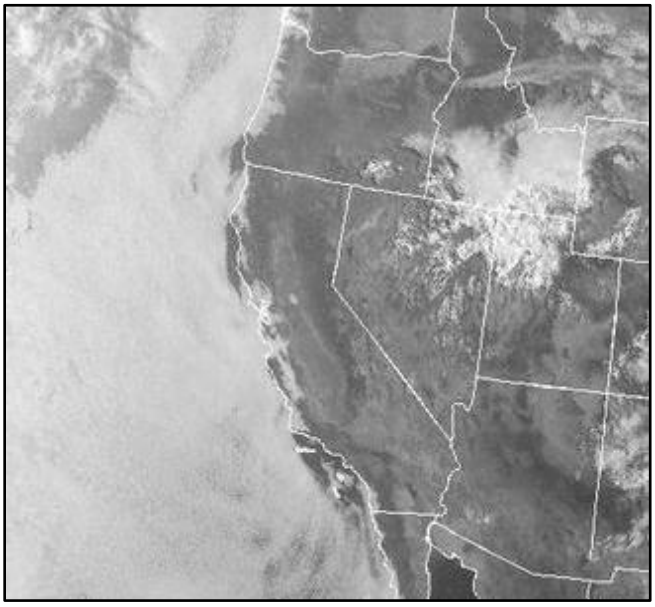

Figure 4.1.5. GOES visible satellite imagery from 29 August 2003 (0745 PDT).

Finally, HYSPLIT 72- hour backward trajectories from NARR data were used from the time and location of the Devil Fire to identify the source region of the dry air. Figures 4.1.6 and 4.1.7 indicate an origin almost 2000 km to the northwest over the Pacific Ocean and a slow descent from an initial altitude of 4000 m MSL to a final elevation of 1000 m MSL. Such results are consistent with synoptic composite analysis that show an offshore source region associated with large-scale subsidence.

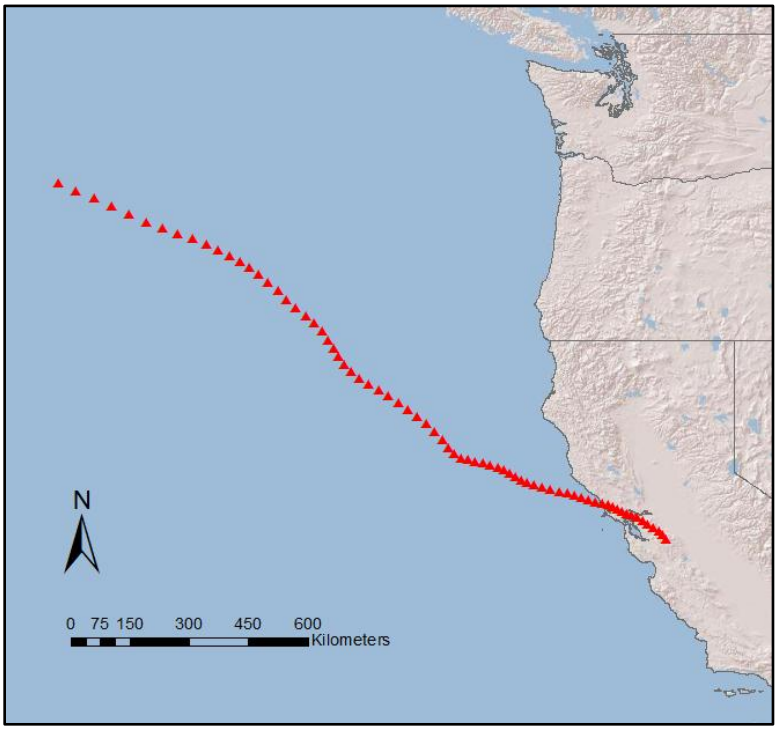

Fig. 4.1.6. 72 hr HYSPLIT horizontal backward trajectory from Devil Fire shelter deployment site.

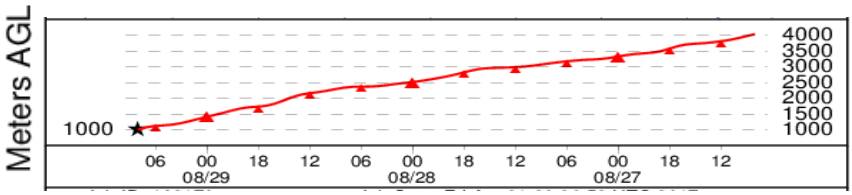

Fig. 4.1.7. 72 hr HYSPLIT vertical backward trajectory from Devil Fire shelter deployment site.

4.3 Numerical Simulation

An overview of the larger scale meteorological features that contributed to the surface drying conditions during the fire shelter deployment is shown through WRF simulations in Fig. 4.2.1. At the 500 hPa level on 28 August 1500 PDT, a trough of low pressure is evident off the California coast with an axis along 124°W (Fig. 4.2.1a). Within the southwesterly flow over California, a streak of relatively dry air is stretched across the SFBA, while downstream there is a local maximum of dry air over the southern Sierra Nevada and southwestern Nevada. At 0100 PDT on 29 August, a closed low is situated over northern California with broad cyclonic flow around the state that drops southeastward into central California by the afternoon (Fig. 4.2.1d,g).

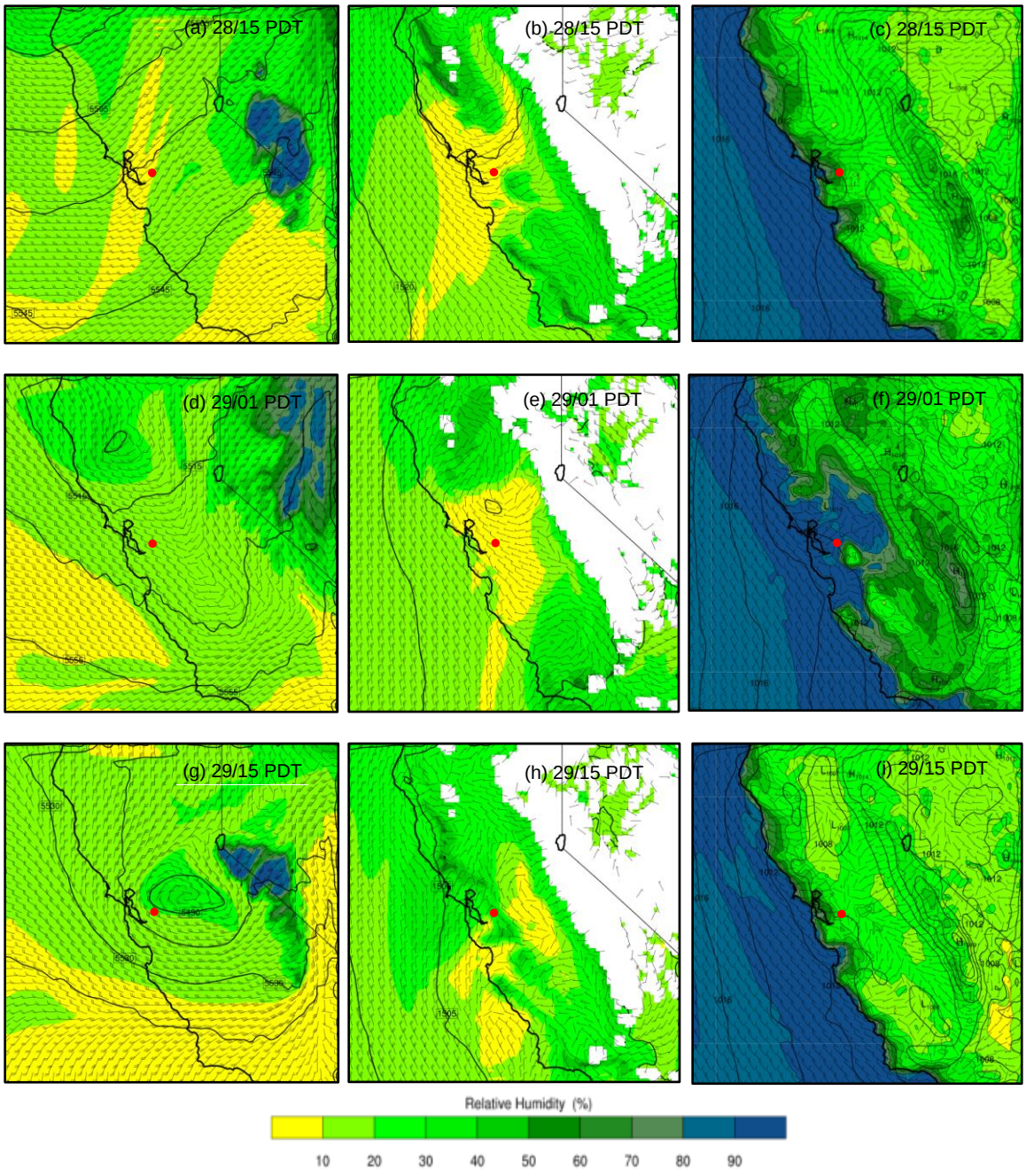

Fig. 4.2.1. Relative humidity (shaded), heights (contours), and winds (barbs) (m s^{-1}) at 500 hPa (left), 850 hPa (center), and the surface (right) for 28 August 1500 PDT, 29 August 0100 PDT and 29 August 1500 PDT. The approximate location of the Devil Fire shelter deployments is represented by a red dot.

The 850 hPa evolution shows a patch of RH below 10% along the central California coast, extending south of Point Arena in a wedge-like shape to 34°N and 124°W, intruding through coastal gaps in the SFBA, and into the Sacramento Valley (Fig. 4.2.1b). At the time of the Devil Fire NDE, the back edge of the 850 hPa dry air source was located over the Diablo Range in northwesterly flow (Fig. 4.2.1e). Simultaneously, surface RH values greater than 90% represent a marine layer over the coastal waters and along the California coast, extending into coastal valleys and through gaps in the Coast Range (Fig. 4.2.1f). Islands of lower RH values outline the terrain above the marine layer while more evenly distributed values are found during the afternoon on 28 and 29 August (Fig. 4.2.1c,f,i).

For the same times as above (28/1500 PDT, 29/0100 PDT, 29/1500 PDT), vertical cross sections through the location of the Devil Fire aligned perpendicular to the Diablo Range at 1 km resolution (Line 1) and parallel to the Diablo Range in 3 km resolution (Line 2) were used to diagnose moisture and potential temperature characteristics in the vertical (Fig. 4.2.2). Results displayed in Fig. 4.2.3a show a layer of dry air with RH less than 10% and dew points below -10°C above a marine layer advecting over the Santa Cruz Mountains and onto the western slopes of the Diablo Range at 1500 PDT on 28 August. At 0100 PDT that night, the dry layer has advected into the eastern slopes of the Diablo Range, as well as the western portion of the Central Valley (Fig. 4.2.3c). Humidity recoveries the following afternoon increase above 25%, with patches of drier air remaining over the coastline and Central Valley (4.2.3e).

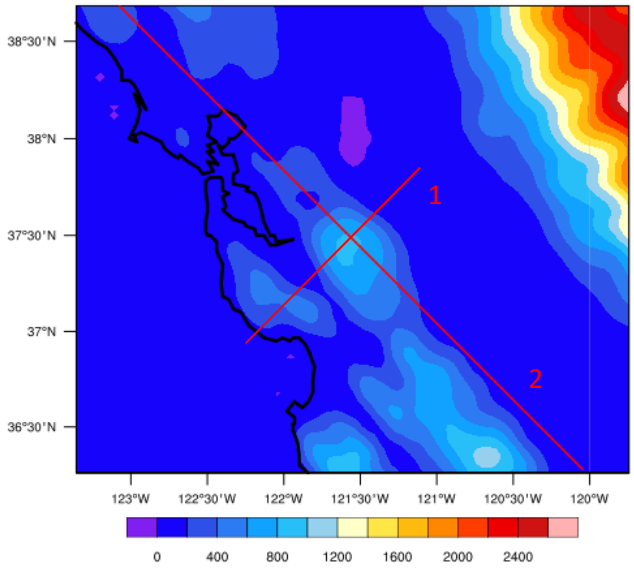

Fig. 4.2.2. SW-NE cross section through domain 3 (Line 1) and NW-SE cross section through domain 2 (Line 2) intersecting at the fire shelter deployment site.

There is a link between boundary layer depth and moisture in the upper elevations. The inversion height, as represented by the strongest potential temperature gradient, remains fairly constant along the coast between night and day, but fluctuates over mountains and valleys (Fig. 4.2.3b,d). The boundary layer depth increases in the mountains during the day as thermally-driven circulations decrease stability and advect air with greater moisture values up-slope (Fig4.2.3a-e). At night, as the boundary layer cools and thermally-driven up-slope circulations cease, the inversion and associated dry air aloft decrease in altitude (Fig. 4.2.3c,d). Gravity waves are also resolved in the numerical solution propagating upstream in subcritical flow (Fig. 4.2.3b) and downstream in supercritical flow (Fig. 4.2.3f).

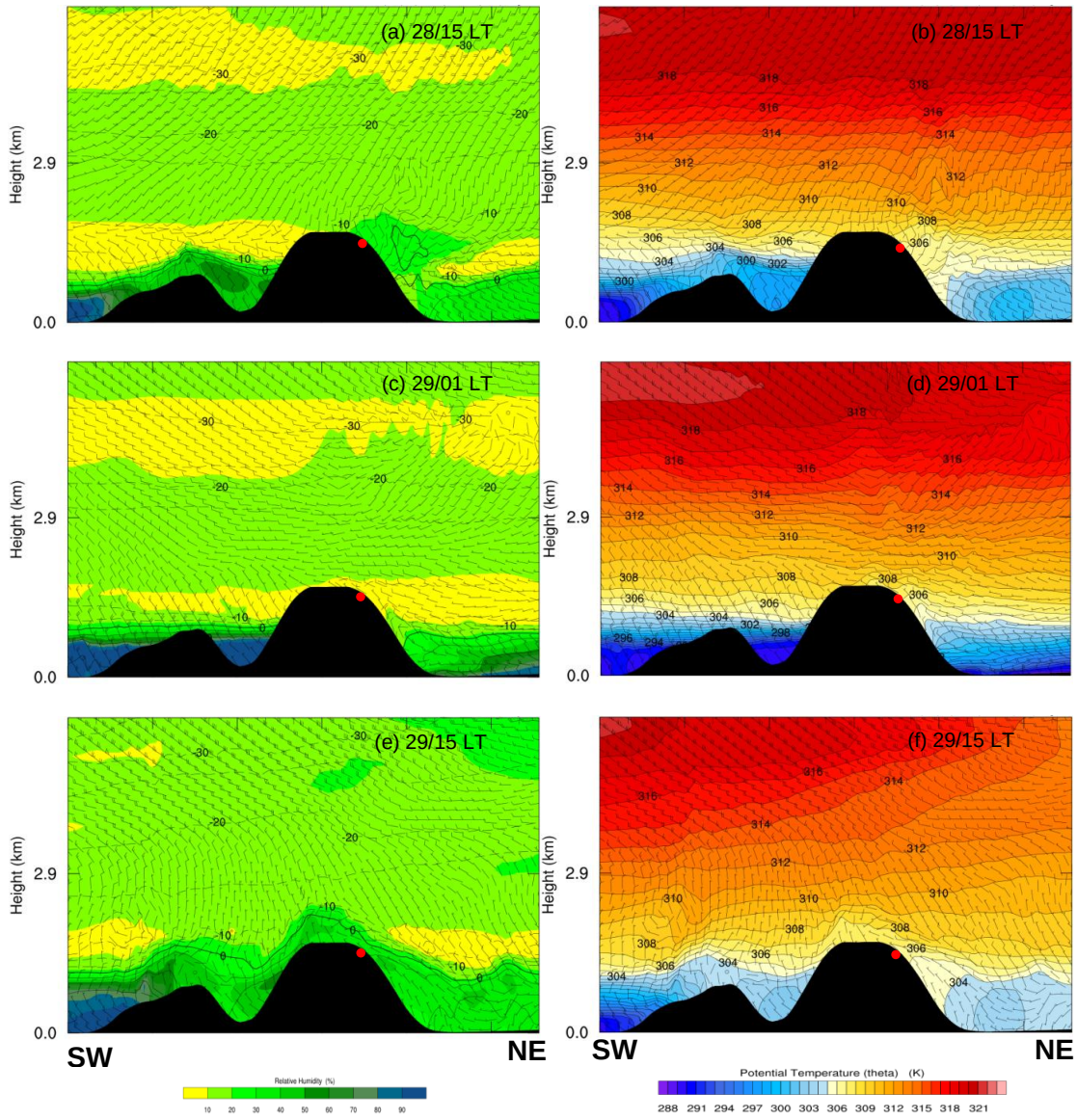

Fig. 4.2.3. Southwest to northeast cross sections across the Diablo Range (Line 1) of relative humidity (shaded) dew point (contours), horizontal winds (m s^{-1}) (left) and potential temperature (shaded) and horizontal winds (m s^{-1}) (right). The approximate location of the Devil Fire shelter deployments is represented by a red dot.

Cross-sections from the northwest to southeast of the same variables display similar results. A thin strip of dry air advects from the west-northwest, over the SFBA and across the Diablo Range at night, then dissipates the following afternoon (Fig. 4.2.4a,c,e). There is a general tilt in isentropes from north to south that is more pronounced across the north on 28 August (Fig. 4.2.4b) and across the south that night (Fig. 4.2.4d) as the short wave trough passed through. This represents descending motions in the atmosphere from west to east and north to south in the area around the Devil Fire.

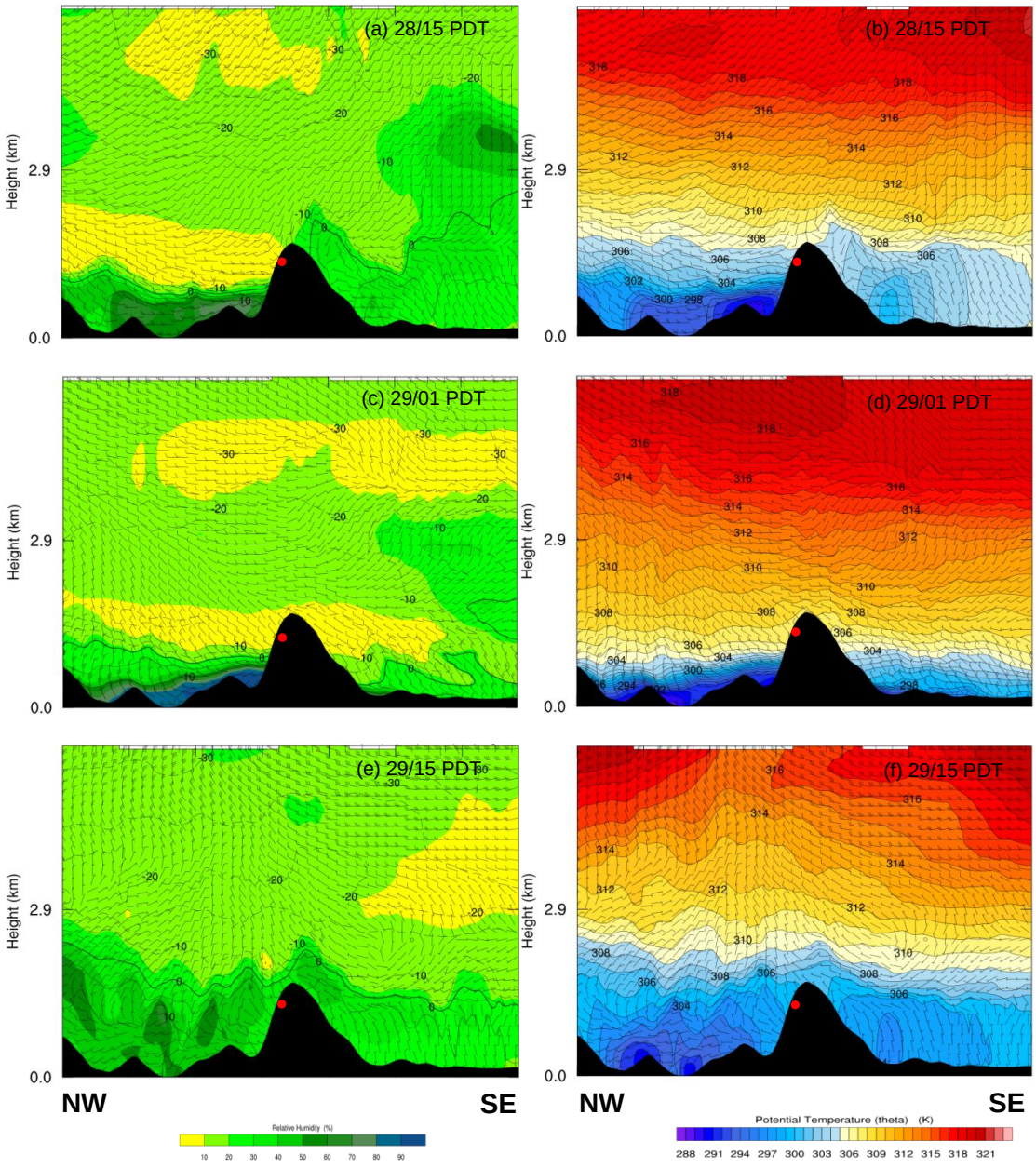

Fig. 4.2.4. Same as 4.2.3 except for a northwest to southeast cross section (Line 2)

While the WRF model captured the layer of dry air above a marine inversion successfully, interpolated surface variables from the site of the Devil Fire shelter deployment site matched poorly to observed conditions from RSP (Fig. 4.2.5 and 4.2.6). Simulated temperature values compare well to actual values and follow appropriate diurnal cycles, but simulated moisture variables display opposite trends compared to observations. Model dew point temperatures follow a diurnal pattern similar to temperature, therefore producing highest RH values at night and lowest values during the day, opposite of what actually occurred. Resolving interactions between terrain and surface meteorological conditions in numerical simulations is important in the complex terrain of the SFBA. Small changes in elevation can mean dramatically different fire danger or behavior.

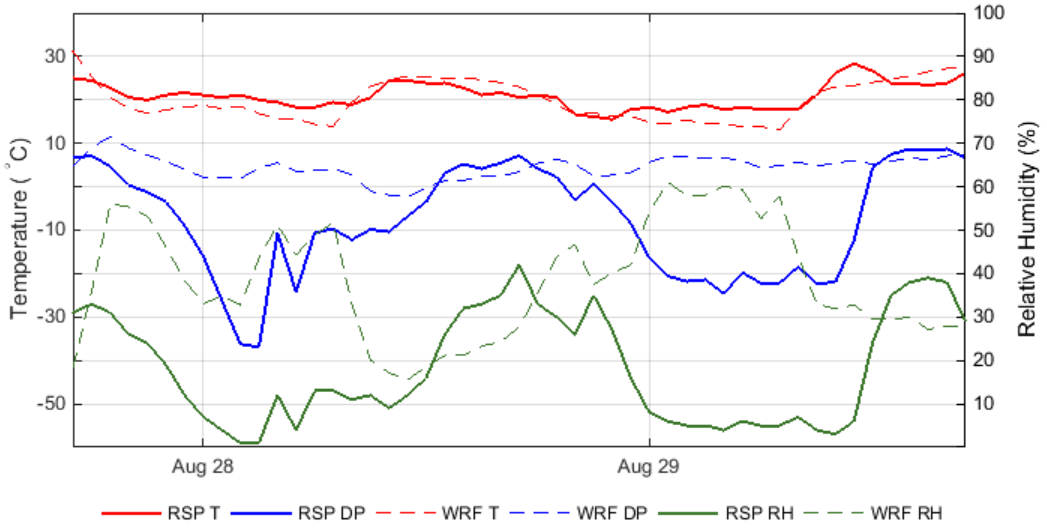

Fig. 4.2.5. Time series of temperature and moisture variables from RSP and interpolated WRF values from the Devil Fire shelter deployment site on 28 and 29 August 2003.

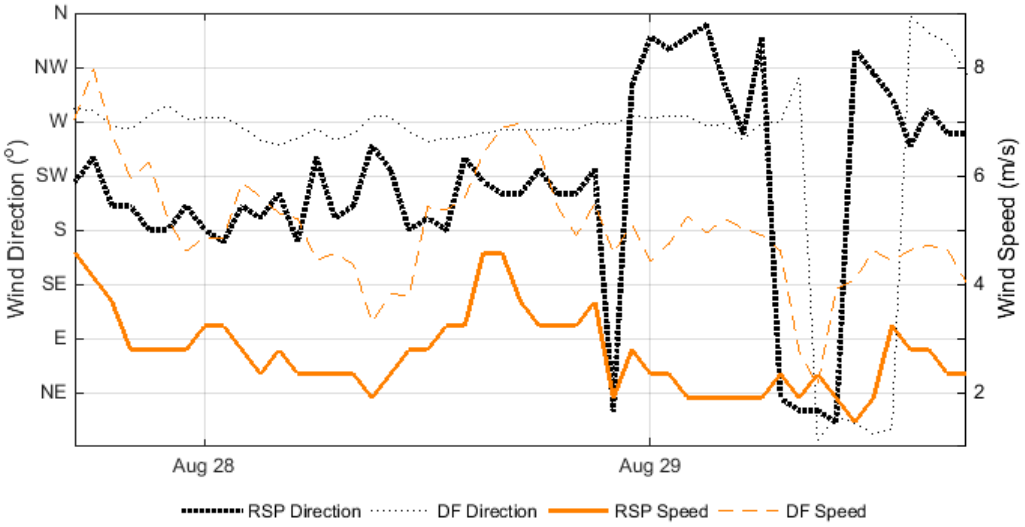

Fig. 4.2.6. Same as 4.2.5 except for wind speed and direction.

Overall, the WRF model system performed satisfactorily in capturing the meteorological conditions surrounding the emergency fire shelter deployment during the Devil Fire. A relatively weak upper-level trough of low pressure is depicted moving

across northern California. In the lower levels, a source of dry air is present near the coast and above a moist marine layer that advects inland prior to deployment. That night, as winds transitioned from westerly to northwesterly and the boundary layer decoupled, extremely dry air reached the surface of slopes above 800 m MSL.

WRF experiments revealed the most important feature during NDEs are boundary layer processes responsible for such dry air reaching the upper slopes of coastal topography. Dry air may be present 925 and 850 hpa levels during the day, but it does not descend upon the surface of elevated terrain until nighttime. This is due to thermally-driven upslope winds during the daytime that advect air from higher moisture environments in the lower slopes to the dry upper slopes. Warmer air is also advected upslope that deepens the terrain-following boundary layer and lifts the inversion off the surface. As surface heating and corresponding circulations cease after sunset, the inversion and associated dry air aloft are able to settle at or below ridgelines.

5. Summary and Conclusion

An abrupt and dramatic overnight decrease in RH resulted in the explosive growth of a wildfire that overran crews and forced the largest fire shelter deployment in California history during the Devil Fire on 29 August 2003. The location was near the SFBA in a remote area of the Diablo Range, a rugged mountain chain that extends down the interior coastal region of central California. Higher coastal elevations across central California are plagued by episodes of severe and often sudden onsets of nocturnal drying. Relative humidity values below 0.5%, dew point temperatures of -40°C, and mixing ratios less than 0.5 g kg^{-1} have been measured in these elevated locations. Nocturnal drying events

are a major concern for firefighting agencies because they pose a great threat to fire behavior, but are poorly understood.

A basic set of qualifications based on the meteorological conditions during the Devil Fire blow-up was used to identify and investigate such events (RH < 9.5% and dew point temperatures <= -10°C for at least 3 hours between 2000-0800 PDT). A climatology identified the spatial and temporal extent of NDEs in California and Oregon. Synoptic compositing of pressure levels and upper air soundings revealed the larger scale mechanisms leading to the formation of dry air and event evolution. Finally, a detailed case study was performed in the 24 hours surrounding of the Devil Fire shelter deployment. Key findings from this study include:

- A source region of extremely dry air at the 850 hPa level associated with large-scale subsidence over the northeastern Pacific. Subsidence is enhanced by an elongated LLJ in an area within a few hundred kilometers of the California coast.
- The dry air exists in a layer above the marine inversion and they both advect inland overnight. An upper-level trough of low pressure amplifying along the west coast of the U. S. promotes onshore advection and is associated with periods of significant nocturnal drying in upper elevations.
- Events are more pronounced in the higher elevations of the SFBA where gaps are present in the coastal barrier, but are common throughout California coastal terrain south of 40°N.

A synoptic composite of 87 significant NDEs from the SFBA reveals key features in large scale dynamics responsible for the formation of dry air and how NDEs evolve. Surface high pressure over the northeastern Pacific and a thermal low pressure area in the southwest U. S. create a baroclinic marine inversion off the California coast. A LLJ develops above this inversion, creating substantial divergence at the 925 hPa level, subsidence in the lower troposphere, and strengthening of the marine inversion. A source region of dry air at 850 hPa accompanies this region of low-level divergence, an extension of which advects through coastal barriers with the marine layer overnight. More significant NDEs are associated with an inland push of stratus and cooler temperatures as a weak upper-level short wave trough of low pressure moves across the Pacific Northwest, causing the eastern Pacific subtropical high and thermal trough along the West Coast to deteriorate. Furthermore, upper-level convergence aloft associated with the approaching low pressure trough enhances subsidence over the SFBA while ushering in a separate source of dry in the middle troposphere from latitudes south of 35°N.

A strong inversion separates the marine layer from extremely dry air aloft. Depending on the height of this inversion and speed of the background wind, supercritical flow is possible near ridge crest levels that accelerate winds and generate gravity waves over leeward slopes. The inversion acts as a thin interface between benign and critical fire conditions and fluctuates over time. During the day, thermal circulations increase the boundary layer depth and vent higher-moisture air into upper elevations. At

night when upslope flow ceases, the boundary layer decouples and dry air is able to reach the surface of upper elevation slopes.

There are many characteristics to nocturnal drying. The events covered in this paper portray some of the more drastic conditions, but nighttime drying events exhibit much variation. Figure 4.5.1 is an idealized conceptual model showing how dry air above a moist marine layer intrudes inland and collapses upon higher terrain at night.

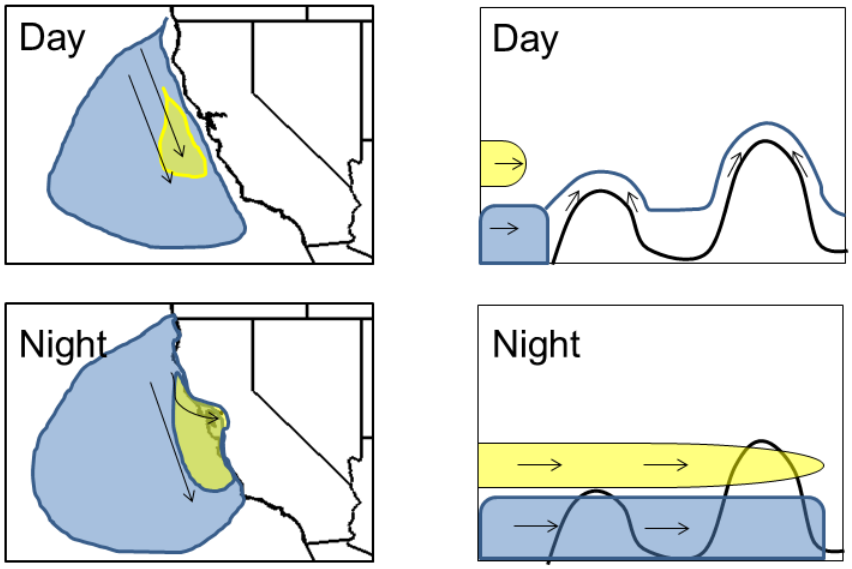

Fig. 4.3.1. Conceptual model of NDEs. Blue shading represents cool, moist marine air and yellow shading represents warm and dry air aloft. Arrows are generalized wind vectors.

Overall, NDEs are more pronounced in coastal terrain above 800 m MSL south of Point Arena, but are possible as low as 450 m MSL. Event duration can last from an hour at a minimum or persist all night and some cases can continue for several consecutive nights. The threat of nocturnal drying is ignored by daily NFDRS ratings and a need exists to further quantify and forecast NDEs. High resolution numerical models are successful in capturing NDEs, but can be improved with better terrain resolution and initial boundary conditions, especially over the northeastern Pacific where in situ measurements are rare. This paper showed a transition from very low to extreme fire danger can occur overnight and NDEs are a common summertime feature in the elevated terrain of coastal California.

References

Beals, E. A., 1914: The value of weather forecasts in the problem of protecting forests from fire. *Monthly Weather Review*, **42**, 111-119.

Bridger, A. F. C., W. C. Brick, and P. F. Lester, 1993: The structure of the marine inversion layer off the central California coast: mesoscale conditions. *Monthly Weather Review*, **121**, 335-351.

Brotak, E. A., and W. E. Reifsnyder, 1977: An investigation of the synoptic situations associated with major wildland fires. *Journal of Applied Meteorology*, **16**, 867-870.

Burk, S. D. and W. T. Thompson, 1996: The summertime low-level jet and marine boundary layer structure along the California coast. *Monthly Weather Review*, **124**, 668-686.

_____ and T. Haack, 2000: The dynamics of wave clouds upwind of coastal orography. *Monthly Weather Review*, **128**, 1438-1455.

Brewer, M. C., Mass, C. F., Potter, B., 2012: The West Coast thermal trough: climatology and synoptic evolution. *Monthly Weather Review*, **140**, 3820-3842

California Department of Forestry and Fire Protection, 2003: Wildland Fire Entrapment Fire Shelter Deployment Review. CA-SCU-003581. 8pp.

Dorman, C. E.,Holt, T., Rogers, D.P., Edwards, K., 2000: Large scale structure of the June-July 1996 marine boundary layer along California and Oregon. *Monthly Weather Review*, **128**, 1632-128.

Fosberg, M. A., Schroeder M. J., 1965: An example of nighttime drying in the Santa Ana Mountains. U. S. Forest Service Research Note PSW-74. 6pp.

Edinger, J. G., 1959: Change in the depth of the marine layer over the Los Angeles basin. *Journal of Meteorology*, **16**, 706-712.

_____, 1963: Modification of the marine layer over coastal southern California. *Journal of Applied Meteorology*, **2**, 706-712.

Huang, C., Y. -L. Lin, M. L. Kaplan, and J. J. Charney, 2009: Synoptic-scale and mesoscale environments conducive to forest fires during the October 2003 extreme fire event in southern California. *Journal of Applied Meteorology and Climatology*, **48**, 553-579.

Kaplan, M. L., C. Huang, Y. -L. Lin, and J. J. Charney, 2008: The development of extremely dry air due to vertical exchanges under the exit region of a jet streak. *Meteorology and Atmospheric Physics*, **102**, 63-85.

Kondo, J. and T. Kuwagata, 1992: Enhancement of forest fires over northeastern Japan due to atypical strong dry wind. *Journal of Applied Meteorology*, **31**, 386-396.

Leiper, D. F., 1948: Fog development at San Diego, California. *Journal of Marine Research*, **7**, 337-346.

Lester, P. F., 1985: Studies of the marine inversion over the San Francisco Bay Area… a summary of the work of Albert Miller, 1961-1978. *Bulletin of the American Meteorology Society*, **66**, 1396-1402.

Mass, C. F. and M. D. Albright, 1987: Coastal southerlies and alongshore surges of the west coast of North America: evidence of mesoscale topographically trapped response to synoptic forcing. *Monthly Weather Review*, **115**, 1707-1738.

_____ and _____, 1989: Origin of the Catalina eddy. *Monthly Weather Review*, **117**, 2406-2436.

McCarthy, E. F., 1923: Forest fire weather in the Southern Appalachians. *Monthly Weather Review*, **51**, 182-185.

Mills, G. A., 2008: Abrupt surface drying and fire weather part 1: overview and case study of the South Australian fires of 11 January 2005. *Australian Meteorology Magazine*, **57**, 299-309.

_____, 2008: Abrupt surface drying and fire weather part 2: a preliminary synoptic climatology in the forested areas of southern Australia. *Australian Meteorology Magazine*, **57**, 311-328.

Munns, E. N., 1921: Evaporation and forest fires. *Monthly Weather Review*, **49**, 149-152.

Neiburger, M., 1960: The relation of air mass structure to the field of motion over the eastern North Pacific Ocean in summer. *Tellus*, **12**, 31-40.

Nimchuk, N., 1983: Wildfire behavior associated with upper ridge breakdown. *Alberta Energy and Natural Resources Forest Service*, Report Number T/50.

Noonkester, V. R., 1979: Coastal marine fog in southern California. *Monthly Weather Review*, **107**, 830-851.

Petterssen, S., 1938: On the causes and the forecasting of the California fog. *Bulletin of the American Meteorology Society*, **19**, 49-55.

Pilié, R. J., E. J. Mack, C. W. Rogers, U. Katz, and W. C. Kocmond, 1979: The formation of marine fog and the development of fog-stratus systems along the California coast. *Journal of Applied Meteorology*, **18**, 1275-1286.

Sharples, J. J., Mills, G. A., and McRae, R. H. D., 2012: Extreme drying events in the Australian high-country and their implications for brushfire risk management. *Australian Meteorological and Oceanographic Journal*, **62**, 157-169.

Skamarock, W. C., Klemp, J. B., Dudhia J., Gill, D. O., Gill, Barker D. M., Wang, W., and Powers, J. G., 2008: A description of the Advanced Research WRF (Version 3). NCAR Technical Note TN-475+STR, 125pp.

Sommers, W. T., 1978: LFM forecast variables related to Santa Ana wind occurrences. *Monthly Weather Review*, **106**, 1307-1316.

Schroeder, M. J., 1960. Humidity patterns at middle elevations in the coastal mountains of southern California. USDA Forest Service, Pacific Southwest Forest and Range Experiment Station. 6 pp.

_____, M. Glovinsky, V. F. Hendricks, F. C. Hood, M. K. Hull, H. L. Jacobson, R. Kirkpatrick, D. W. Kreuger, L. P. Mallory, A. G. Oertel, R. H. Reese, L. A. Sergius, C., E. Syverson, 1964: Synoptic weather types associated with critical fire weather. USDA Forest Service, Pacific Southwest Forest and Range Experiment Station. 492 pp.

Werth, P. A., B. E. Potter, C. B. Clements, M. A. Finney, S. L. Goodrick, M. E. Alexander, M. G. Cruz, J. A. Forthofer, S. S McCallister, 2011: Synthesis of knowledge of extreme fire behavior: volume I for fire managers. USDA Forest Service, Pacific Northwest Research Station. 144pp.

Whiteman, 2000: Mountain meteorology: fundamentals and applications. Oxford University Press. 355pp.

Walbrun, R, and Blier, W., cited 2004: An examination of a lightning event in the San Francisco Bay region using the weather event simulator. WFO Monterey, CA, April 2017 [Available online at www.weather.gov/media/wrh/online_publications/talite/talite0425.pdf].

Zimet, T., J. E. Martin, and B.E. Potter, 2007. The influence of an upper-level frontal zone on the Mack Lake Wildfire environment. *Meteorological Applications*, **14**, 131-147.